Linear and Third-Order Nonlinear Optical Properties of Fe(eta(5)-C5Me5)(kappa(2)-dppe)- and trans-Ru(kappa(2)-dppe)(2)-Alkynyl Complexes Containing 2-Fluorenyl End Groups

Amédée Triadon, Guillaume Grelaud, Nicolas Richy, Olivier Mongin, Graeme J. Moxey, Isabelle M. Dixon, Xinwei Yang, Genmiao Wang, Adam Barlow, Joelle Rauh-Berthelot, et al.

Linear and Third-Order Nonlinear Optical Properties of Fe(η^5-C_5Me_5)(κ^2-dppe)- and *trans*-Ru(κ^2-dppe)$_2$-Alkynyl Complexes Containing 2-Fluorenyl Endgroups

Amédée Triadon,[a] Guillaume Grelaud,[a,b] Nicolas Richy,[a] Olivier Mongin,[a] Graeme J. Moxey, [b] Isabelle M. Dixon,[c] Xinwei Yang,[b] Genmiao Wang,[b] Adam Barlow,[b] Joelle Rault-Berthelot,[a] Marie P. Cifuentes,[b] Mark G. Humphrey,[b,] and Frédéric Paul[a,]**

[a] Univ Rennes, CNRS, *ISCR (Institut des Sciences Chimiques de Rennes)*, UMR 6226, F-35000 Rennes (France).

[b] Research School of Chemistry, Australian National University, Canberra, ACT 2601 (Australia).

[c] *Laboratoire de Chimie et Physique Quantiques*, Université de Toulouse, CNRS, F-31062 Toulouse, France.

ABSTRACT: *The synthesis and characterization of a set of redox-active iron and ruthenium alkynyl complexes of general formula [[M]Cl$_{(1-p)}${C≡CC$_6$H$_{5-m}$(C≡CFlu)$_m$}$_{(1+p)}$][PF$_6$]$_n$ are reported (n = 0-1; m = 1-2; [M] = [Fe(η^5-C$_5$Me$_5$)(κ^2-dppe)] and p = 1 or [M] = [trans-Ru(κ^2-dppe)$_2$] and p = 0-1). The linear and third-order nonlinear optical properties of these new organometallic complexes featuring phenylalkynyl ligands functionalized by 2-fluorenyl (Flu) groups were studied in their stable redox states. Their first electronic transitions are assigned with the help of DFT calculations. We show here that these compounds possess significant third-order NLO responses in the near-IR range for molecules of their size. In particular, the remarkably large 2PA activities of the new Ru(II) compounds in the 600-800 nm range (Z-scan) make them attractive nonlinear chromophores. Structure-property studies emphasize the importance of para- vs. meta- connection of the 2-fluorenylethynyl units on the phenylalkynyl core, and also reveal that upon progressing from mono- to bis-alkynyl complexes, a further increase of the 2PA cross-section can be obtained while maintaining linear transparency in the visible range.*

INTRODUCTION

Among redox-active inorganic chromophores,[1] iron(II) or ruthenium(II) alkynyl complexes were identified very early as outstanding electrophores,[2-3,4] with potential in diverse fields ranging from photovoltaic conversion[5,6] to electroluminescent displays.[7,8-11] A large part of this promising potential in molecular photonics rests on their remarkable electrochromism, which extends to their nonlinear[12-13,14-17] and chiroptical properties.[18,19]

The fluorenyl unit, with its high fluorescence quantum yield[20] and large multi-photon absorption cross-section,[21] is indeed an interesting building block for the construction of molecular arrays endowed with photonic properties.[22] It was therefore of significant interest to study alkynyl complexes featuring 2-fluorenyl endgroups, a class of compounds that has been curiously overlooked

in the literature.[23] In this context, we have recently reported series of [Fe(η^5-C_5Me_5)(κ^2-dppe)]-based[24] and [*trans*-Ru(κ^2-dppe)$_2$]-based complexes[25] such as **1a-b**, **2a** and **3** (Chart 1).[26]

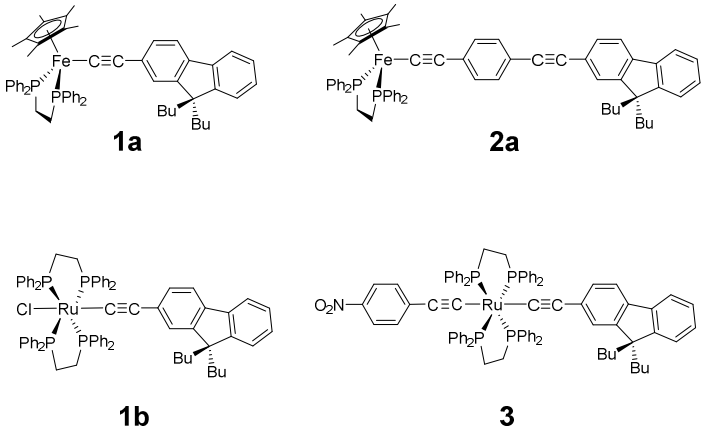

Chart 1. Extant 2-Fluorenyl-based Alkynyl Complexes.

Consistent with other alkynyl complexes,[14,17,27] 2-ethynylfluorenyl complexes possess strong third-order NLO responses around 800 nm,[12] and if sufficient luminescence could be coupled to their NLO properties (specifically two-photon absorption), these compounds would have significant applications potential.[28] Unfortunately, when excited at wavelengths around 300 nm, many of these d^6-metal alkynyl complexes were found to be (at best) weakly emissive, with luminescence quantum yields of a few percent (e.g. < 1 % for **1a-b**), regardless of their redox state.[24-25] The origin of this emission remains unclear, a fluorene-centred (LC) excited state being suspected to be responsible instead of the lower-lying MLCT or LMCT excited states, but in contrast to hypotheses found in the literature,[9-11] oxidative trapping of the excited fluorene LC state by the first MLCT state does not account for the fluorescence quenching in the M(II) complexes **1a-b** and **3** (M = Fe, Ru).[25]

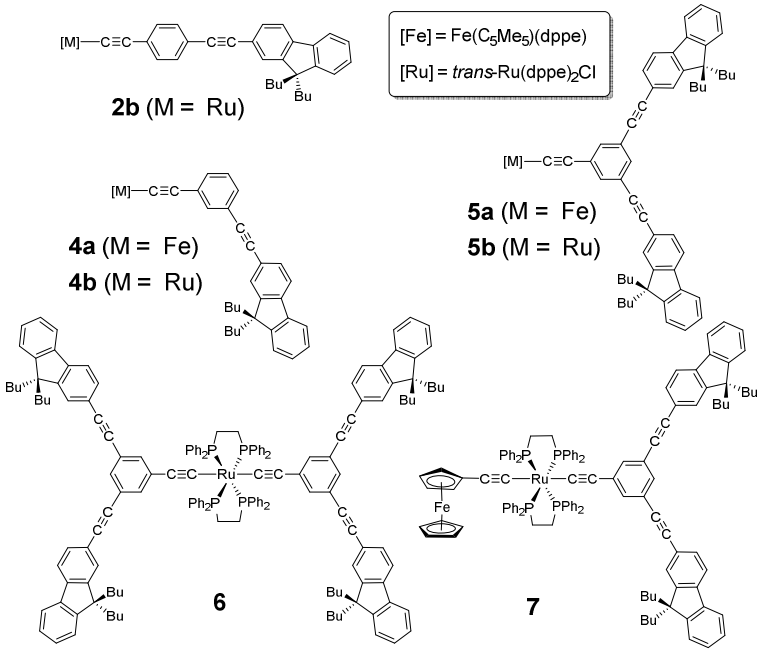

Chart 2. Target 2-Fluorenyl-based Alkynyl Complexes.

In order to learn more about the structure- and redox-dependence of the photonic properties of these fluorenyl-containing ruthenium and iron alkynyl complexes, we now report the synthesis of several additional examples (Chart 2). Compared to the known complexes, the new derivatives possess extended alkynyl ligands containing one (**2b**, **4a-b**) or more (**5a-b**, **6**-**7**) 2-ethynylfluorenyl unit(s). These structural variations will allow probing of the effect of meta vs. para connection on their luminescence properties. Thus, for a given organometallic endgroup, the para (**2a-b**) vs. meta (**4a-b**) isomers should exhibit significant differences in electronic coupling (H_{ab}) between the redox endgroups involved in the redox quenching process.[29]

Indeed, we have shown with closely related organoiron mixed-valent complexes that the electronic coupling is reduced by an order of magnitude proceeding from para- to meta-connected diethynylphenylene-bridged complexes.[30-31] Also, replacement of [Fe(η^5-C_5Me_5)(κ^2-dppe)] by the more electronegative [*trans*-Ru(κ^2-dppe)$_2$Cl] in a given compound changes the thermodynamic driving force and activation energy for the redox-quenching process of the fluorescent LC state.[25] Such changes will impact the kinetics of the redox-quenching process (k_{eT}) according to eqs 1-3 and, if this process dominates the non-radiative deactivation rate, they should in turn influence the luminescence quantum yields in a predictable way.[32]

$$\Phi_{lum} = k_{lum}/(k_{lum} + k_{eT} + k_{NR}) \quad (1)$$

$$k_{eT} = C(H_{ab})^2 \exp(\Delta G^{\neq}/k_B T) \quad (2)$$

$$\Delta G^{\neq} = (\Delta G_{eT} + \lambda)^2/(4\lambda) \quad (3)$$

Finally, the impact of these structural variations on the third-order NLO properties will also be analyzed for the Ru(II) complexes and compared to corresponding data available for the Fe(II) analogues.[24] In this respect, comparison between **5b** and **6** should also provide information on the influence of symmetry (dipolar vs. quadrupolar) on cubic NLO properties.[34] Complemented by theoretical calculations, this study should therefore contribute to a better understanding of the linear and (third-order) nonlinear optical properties of these d^6/d^5-metal arylalkynyl complexes incorporating 2-fluorenyl endgroups (M = Fe, Ru).

RESULTS

Synthesis and Characterization of the Fe(II) and Ru(II) Complexes. The targeted Fe(II) and Ru(II) mono-alkynyl complexes **2b**, **4a-b** and **5a-b** were synthesized from the known organic alkyne precursors[35] (**8**, **9** and **10**) obtained following a new high-yielding approach (Supporting Information) and the corresponding Fe(II) chloride precursor Fe(η^5-C_5Me_5)(κ^2-dppe)(Cl)[31,36] or Ru(II) triflate precursor [Ru(κ^2-dppe)$_2$Cl][OTf],[37] following classic reactions (Scheme 1).[4,38] The vinylidene intermediates (**2b-v**, **4a/b-v** and **5/b-v**) were isolated and characterized (Supporting Information). The bis-alkynyl Ru(II) complexes **6** and **7** were obtained from *trans*-[Ru(κ^2-dppe)$_2$Cl][PF_6], using either two equivalents of ligand **10** for one equivalent of the Ru(II) precursor (Scheme 2), or by reacting **5b** with a slight excess of ethynylferrocene (Scheme 3).[39]

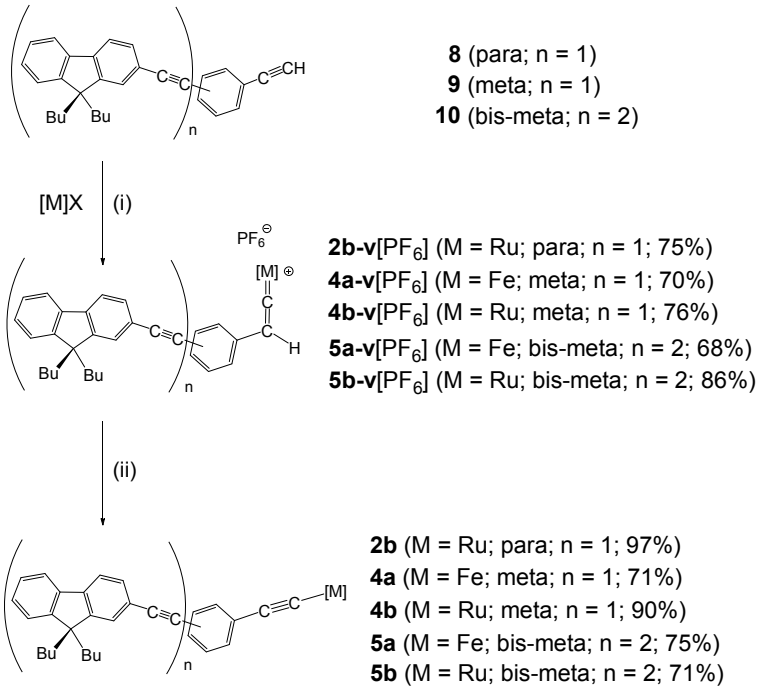

Scheme 1. Synthesis of the M(II) Alkynyl Complexes **2b**, **4a-b** and **5a-b**. (a) M = Fe, X = Cl or PF_6: (i) KPF_6/ MeOH and (ii) ^{t}BuOK/THF. (b) M = Ru, X = PF_6: (i) 40 °C/CH_2Cl_2 and (ii) NEt_3/CH_2Cl_2 ([Fe] = Fe(η^5-C_5Me_5)(κ^2-dppe). [Ru] = *trans*-Ru(κ^2-dppe)$_2$Cl).

All of these orange/red complexes (**2b**, **4a-b** and **5a-b**) were fully characterized, providing the expected ^{31}P NMR signatures for Fe(II)[4] or Ru(II) mono- or bis-alkynyl derivatives.[2,37,39-40] The presence of the triple bond(s) was confirmed by the observation of diagnostic $\bar{\upsilon}_{C\equiv C}$ stretching modes in IR (Supporting Information) and Raman.[15] In addition, **2b, 4b** and **5b** were also characterized crystallographically (Figure 1), featuring usual bonding parameters for such mono-alkynyl Ru(II) complexes (Supporting Information).[37,41-42]

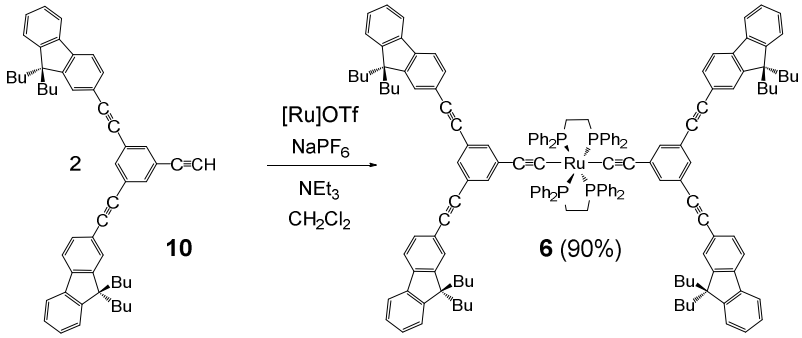

Scheme 2. Synthesis of the Ru(II) Complex **6**.

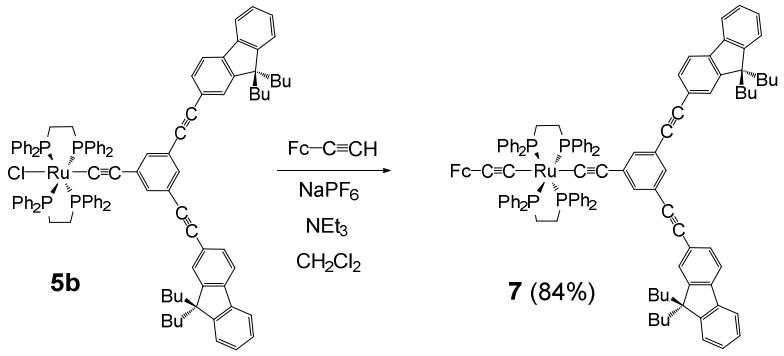

Scheme 3. Synthesis of the Ru(II) Complex **7**.

(a)

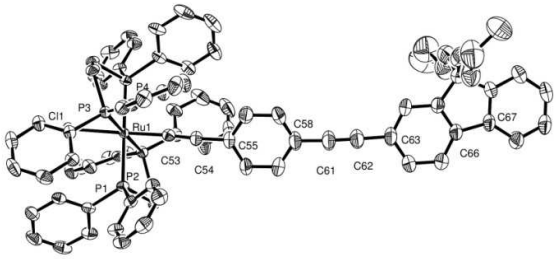

(b)

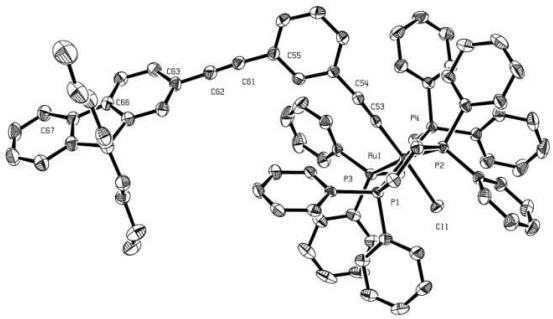

(c)

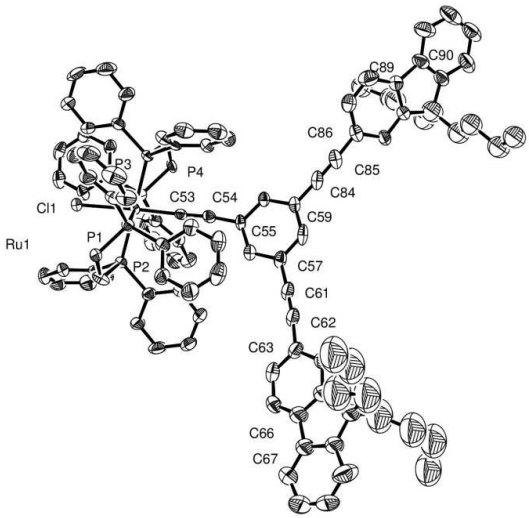

Figure 1. ORTEP representations of 2b (a), 4b (b) and 5b (c) at the 50% probability level.

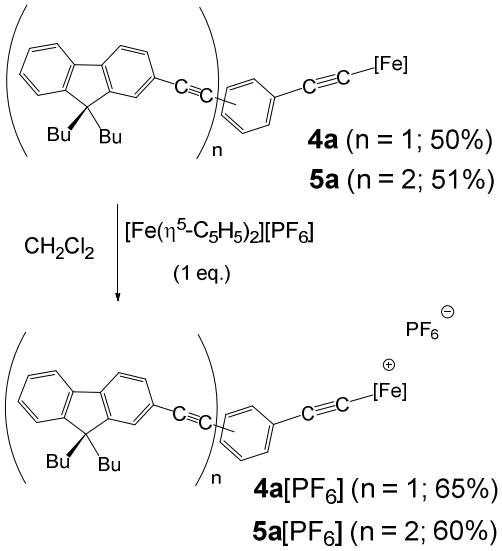

Scheme 4. Synthesis of the Fe(III) Complexes 4a[PF_6] and 5a[PF_6] ([Fe] = Fe(η^5-C_5Me_5)(κ^2-dppe)).

Synthesis and Characterization of the Fe(III) Complexes. The dark green Fe(III) complexes **4a**[PF_6] and **5a**[PF_6] were isolated by chemical oxidation of their Fe(II) parents **4a** and **5a** (Scheme 4). They were characterized by infrared,[43] ESR[24] and ^{1}H NMR spectroscopy[24,44] (Supporting Information), providing the expected signatures for paramagnetic metal-centred radical cations. Thus, rhombic ESR signals were recorded for **4a**[PF_6] and **5a**[PF_6], resembling those previously obtained for **2a**[PF_6][24] or for **11**[PF_6]-**13**[PF_6] (Chart 3).[15,43] Likewise to what has been previously observed for **2a**[PF_6] in ^{1}H NMR, the fluorenyl protons are significantly less shifted than with **1a**[PF_6],[24] consistent with a less marked spin delocalization/polarization on these aromatic units spatially more "remote" from the paramagnetic Fe(III) metal center in **4a**[PF_6] or **5a**[PF_6].

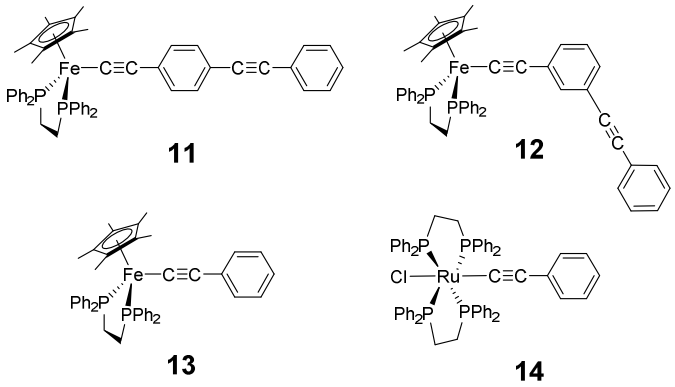

Chart 3. Selected Alkynyl Complexes used as References.

Cyclic Voltammetry Studies. Cyclic voltammograms (CVs) were recorded for **4a** and **5a** (Table 1). Similar to **2a**, their CVs in CH_2Cl_2 reveal a one-electron process at ca. - 0.10 V, corresponding to Fe(II)/Fe(III), which appear chemically reversible at a scan rate of 0.1 V/s. Consistent with published data,[37] the Ru(II) mono-alkynyl analogues **2b**, **4b** and **5b** undergo M(II)/M(III) oxidation at potentials that are ca. 0.60 V higher, while an even higher potential is observed for the bis-alkynyl derivative **6**. The heterobinuclear complex **7** displays two oxidations at positive potentials, one near 0.21 V that is likely attributable to the Fe(II)/Fe(III) oxidation at the ferrocenyl unit, and a second one at 0.82 V,

possibly localized at the Ru(II) center.[45-46] In addition to these chemically reversible processes, irreversible processes are observed above 1.4 V and below -2.0 V for all complexes. These correspond to oxidation and reduction of the fluorene-containing alkynyl ligand, respectively, consistent with the electrochemical behavior of fluorene,[47] 2-ethynyl-9,9-dibutyl-*9H*-fluorene, and the alkynes **8**-**10** (Supporting Information).

Comparing the metal-based oxidations for **2-4a-b** reveals that proceeding from para- to meta-connection of the 2-ethynylfluorenyl substituent induces a very small shift toward more negative potentials (compare **2a** with **4a** or **2b** with **4b**). Expanding the π-manifold of the ligand upon proceeding from **4a** to **5a** or from **4b** to **5b** results in larger (30-60 mV) shifts in the opposite direction, in line with a less facile oxidation of the latter complexes. Compared to oxidation potentials published for Fe(II) phenylethynyl analogues (Table 1), such as **11** (Chart 3)[15] or **12**,[48] these data suggest that 2-ethynylfluorenyl groups are comparable to 4-phenylethynyl groups in terms of electronic substituent influence. In contrast, when directly ligated to the metal center, 2-ethynylfluorenyl appears slightly more electron-releasing than phenylethynyl (compare **1a** and **13**[36] or **1b** and **14)**.[37]

$$\Delta G_{CS1} = E°(D^+/D) - E°(A/A^-) + (Z_A - Z_D - 1)e^2/4\pi\varepsilon_0\varepsilon d \qquad (4)$$

Finally, based on the Rehm-Weller equation (eq. 4),[49] an estimate of the free enthalpy of formation (ΔG_{CS1}) of the intramolecular charge separated state corresponding to the formal transfer of one electron from M(II) toward the fluorenyl ligand (CS1) was derived for all these complexes.[50] These ΔG_{CS1} values are given by the difference between the metal-based oxidation potential and first reduction potential of the fluorenyl-containing ligands (Supporting Information), corrected by the electrostatic term expected in the charge separated species when the positive charge is located on the metal center and the negative charge is located on a fluorenyl group. These values had previously been derived for **1a-b**[25] using the reduction potential reported for fluorene in DMF (-2.89 V vs. SCE)[47] corrected for the change in the dielectric constant of the solvent (*ca.* -3.0 V in the case of CH_2Cl_2). In the present work, we have now determined these potentials by cyclic voltammetry for fluorene, 2-ethynylfluorene, the alkynes **8-10**, and selected complexes (Supporting Information). Our CV measurements suggest that we slightly overestimated the ΔG_{CS1} values of **1a-b** by using the reduction potential of fluorene instead of that of 2-ethynylfluorene. New ΔG_{CS1} values for these compounds have now been calculated using a reduction potential of -2.65 V for the 2-ethynylfluorene in CH_2Cl_2. Indeed, the increased conjugation of the longer ligand appears to exert a significant impact on the reduction potential of the alkyne compared to fluorene, resulting in a decrease of the ΔG_{CS1} value of the complexes **4a-b**, **5a-b** and **6**. Except for **1a** and **1b**, these values are roughly 1 eV below those corresponding to the energies of the first MLCT transitions of the various M(II) complexes expressed in eV (Table 1). Because the onset of the various CT bands is roughly 0.5-0.6 eV below their maximum, the energies of the various CS1 states should be similar to the $\lambda_{0\text{-}0}$ energies of the first MLCT states detected on the spectra. The driving force (ΔG_{eT}) and the activation energy ($\Delta G^{\neq}$) for the electron transfer could then be derived according to eq 3 (See Scheme 5 and Supporting Information).

$$\Delta G_{CS2} = E°(D^+/D) - E°(A/A^-) \qquad (5)$$

Estimates of the free enthalpy of formation (ΔG_{CS2}) of the intramolecular charge-separated state corresponding to the formal transfer of one electron from the fluorenyl ligand to the M(III) center (CS2) were also derived for the Fe(III) complexes **2a**[PF_6]-**5a**[PF_6] using a simplified version of eq. 4 (eq. 5).[51] These ΔG_{CS2} values are given by the difference between the first reduction potential of the fluorenyl-containing ligands and the metal-based reduction potential (Supporting Information). Despite the approximations made in eqs 4 and 5 and the neglect of the electron-electron correlation

energy,[52] the match found between the CS1 (or CS2) deduced from redox data and the energies of the first MLCT (or LMCT) states detected on the electronic absorption spectrum is good for most compounds.

Table 1. Electrochemical Data for the Fe(II) and Ru(II) Alkynyl Complexes.[a]

Cmpd	E^0 (ΔE_p [b])	i_c/i_a	ΔG_{CS1} [c]	E_{MLCT} [d]	Ref.
1a	- 0.17 (0.08)	1	2.28	3.07	this work
			2.63		[25]
2a	- 0.12 (0.08) [b]	1	1.84	2.76	[24]
4a	- 0.13 (0.13)	1	1.95	3.38	this work
5a	- 0.10 (0.07)	1	1.81	2.92	this work
1b	+ 0.41 (0.07)[e]	1	2.86	3.32	this work
			3.21		[25]
2b	+ 0.50 (0.07) [e]	1	2.46	3.09	this work
4b	+ 0.49 (0.07) [e]	1	2.57	<3.61 [f]	this work
5b	+ 0.55 (0.07) [e]	1	2.48	3.40	this work
6	+ 0.57 (0.09) [e]	1	2.48	3.41	this work
7	+ 0.21 (0.08) [e]	1	2.15 [g,h]	3.33	this work
	+ 0.82 (0.08) [e]	~1			
11	- 0.13 (0.09)	1	/	/	[15]
12	- 0.13 (0.08)	1	/	/	[48]
13	-0.15 (0.08)	1	/	/	[36]
14	+0.44 (0.08)	1	/	/	[53]

[a] All E° values given for M(III)/M(II) redox couples are in V vs. SCE. Conditions (unless stated otherwise): CH_2Cl_2 solvent, 0.1 M $[NBu_4][PF_6]$ supporting electrolyte, 20 °C, Pt electrode, sweep rate 0.1 V s^{-1}. Ferrocene/ferrocenium (FcH/FcH^+) was used as an internal reference for potential measurements. [b] Difference between cathodic and anodic peak potentials. [c] Computed (in eV) according to eq. 4 (see text). [d] Energy of the $\pi^*_{Flu} \leftarrow d_M$ (MLCT) state in eV (see Table 2). [e] Measured vs. an AgCl/Ag reference electrode and corrected using Fc as an internal reference. [f] The maximum of the first MLCT peak is hidden below another (LC) peak. [g] Corresponds to a different CS1 state (CS1') in which the Fc and not the Ru(II) site is oxidized. [h] Computed considering an additional 6.4 Å contribution to d relative to **6** in Eq 1, for being oxidized on the Fc rather than on the Ru center.[45]

Absorption Spectroscopy. The UV-Vis-near-IR absorption spectra of the M(II) complexes (M = Fe, Ru) were then recorded in dichloromethane (Table 2). For the Fe(II) complexes, the broad one-photon absorption (1PA) band observed at lowest energy (in the range 400-470 nm) is at the origin of the orange color of these compounds (Figure 2). For **1a** and **2a**, previous TD-DFT calculations indicated that this first band largely consists of a metal-to-ligand charge transfer (MLCT) band,[24] while the next-highest-energy absorption results from the overlap of a second MLCT transition and of a fluorene-centred (LC) transition with apparent vibronic fine structure. Consistent with the involvement of the metal center, the first 1PA band is not found in the absorption spectra of the corresponding organic alkynes, while the second (LC) band occurs at comparable (**4a-b** and **5a-b**) or at slightly higher (**2a-b**) energies. For **4a**, the MLCT absorption is hypsochromically shifted by 81 nm (3719 cm^{-1}) relative to that of **2a** and appears as a shoulder on the $\pi^* \leftarrow \pi$(LC) transition.

Table 2. Absorption and Emission Data for the M(II)/M(III) Complexes in CH_2Cl_2.

Cmpd	Absorption: λ_{max}/nm (10^{-3} ε in M^{-1} cm^{-1})	λ_{em} [λ_{ex}] [a] /nm	E_{em} [b] /eV	Φ_{lum}	Ref.
1a	278 (sh, 33.4), 296 (sh, 30.0), 404 (20.0)	334 [291]	3.71	0.4%	[24]
		507 [403]	2.45	0.2%	
2a [c]	297 (sh, 32.2), 322 (51.0), 336 (sh, 48.9), 448 (28.3)	367 [323]	3.38	0.1%	this work
		≈ 510 [453]	2.43	0.0% [d]	
4a	306 (52.5), 324 (68.7), 340 (59.7), 367 (sh, 22.5)	348 [324]	3.56	0.1%	this work
5a	308 (sh, 64.8), 328 (93.9), 346 (94.5), 425 (9.6)	385 [330]	3.22	0.6%	this work
1b	251(37.6), 286 (sh, 15.9), 352 (sh, 22.2), 373 (24.9)	331 [290]	3.75	0.8%	[25]
2b	308 (38.7), 319 (39.1), 401 (52.3)	369 [319]	3.36	2.0%	this work
		516 [377]	2.40	0.1%	
4b	308 (sh, 91.3), 327 (125.4), 343 (139.5)	350 [327]	3.54	0.4%	this work
5b	308 (sh, 116.7), 329 (182.2), 346 (197.4), 365 (sh, 21.5)	353 [327]	3.51	0.8%	this work
6	308 (sh, 157.4), 329 (248.3), 346 (266.7), 364 (sh, 56.4)	359 [327]	3.45	2.4%	this work
7	312 (sh, 74.6), 330 (112.7), 346 (118.0), 372 (sh, 17.7)	324 [327]	3.83	0.6%	this work
		428 [388]	2.89	0.1%	
1a[PF_6]	280 (36.9), 327 (sh, 26.5), 406 (8.3), 466 (4.8), 624 (sh, 1.9), 764 (8.1), 1824 (0.18)	332 [291]	3.73	0.8%	[24]
2a[PF_6]	290 (29.3), 346 (48.0), 454 (7.9), 613 (2.9), 756 (5.6),1860 (0.17)	422 [346]	2.94	0.6%	this work
4a[PF_6]	307 (sh, 32.6), 324 (75.8), 343 (66.3), 388 (5.9), 579 (2.7), 671 (3.9), 1866 (0.09)	379 [324]	3.27	0.2 %	this work
5a[PF_6]	309 (sh, 84.4), 328 (123.9), 347 (114.6), 395 (7.2), 582 (3.7), 668 (4.4), 1877 (0.1)	378 [330]	3.28	0.4 %	this work
1b[PF_6]	276 (38.2), 309 (sh, 18.3), 439 (16.8), 454 (sh, 12.7), 640 (3.5), 902 (14.5)	ND [e]	/	ND [e]	[25]
2b[PF_6]	274 (64.6), 334 (50.5), 389 (27.0), 489 (sh, 22.0), 507 (25.3), 694 (5.9), 939 (27.3)	ND [e]	/	ND [e]	this work
4b[PF_6]	281 (105.4), 326 (103.6), 346 (102.1), 372 (sh, 19.8), 589 (6.3), 860 (20.0)	ND [e]	/	ND [e]	this work
5b[PF_6]	282 (112.7), 332 (158.2), 349 (152.7), 387 (18.2), 590 (3.2), 879 (18.2)	ND [e]	/	ND [e]	this work
6[PF_6]	312 (123.0), 332 (202.8), 351 (215.8), 397 (16.1), 631 (3.2), 961 (sh, 8.5), 1061 (21.5), 1153 (sh, 17.6)	ND [e]	/	ND [e]	this work
7[PF_6]	312 (62.9), 331 (96.9), 349 (120.0), 421 (sh, 3.7), 569 (7.8), 1557 (5.2), 2300 (5.0)	ND [e]	/	ND [e]	this work
7[PF_6]$_2$	281 (51.9), 312 (51.9), 336 (81.2), 353 (85.4), 399 (12.6), 451 (6.3), 658 (3.1), 1032 (13.0)	ND [e]	/	ND [e]	this work
8	311 (sh, 32.7), 331 (53.5), 352 (54.6)	380 [331]	3.26	58.4%	[24]
9	305 (sh, 31.1), 325 (45.4), 341 (44.9)	350 [323]	3.54	75.8%	this work
10	309 (sh, 62.3), 327 (96.9), 346 (103.6)	359 [327]	4.01	74.2 %	this work

[a] Emission [excitation] wavelengths. [b] Energy of emission. [c] Extinction coefficients redetermined. [d] Not detected. [e] Not determined.

This shift can be attributed to the meta-connection of the 2-fluorenylethynyl substituent in the former complex which somewhat disrupts conjugation through the π-manifold compared to the para-connection in **2a** (Figure 2). Upon progressing from **4a** to **5a**, the MLCT band is shifted bathochromically by 51 nm (3219 cm^{-1}), this shift being induced by the extension of the π-manifold on the alkynyl ligand.

The same observations can be made for the MLCT transition at lowest energy of the Ru(II) analogues **2b**, **4b** and **5b**, except that the hypsochromic shift of the MLCT band between **2b** and **4b** is much larger (4216 cm^{-1}) so that this band remains hidden beneath the LC transition in **4b**. Extending the π-manifold upon progressing from **4b** to **5b** shifts this band bathochromically, but not sufficiently to become fully resolved in the spectrum. As a result, this MLCT band appears as a shoulder on the low-energy side of the LC band. The extinction coefficients of this LC band in **4b** and **5b** are larger than those for the corresponding absorptions in **4a** and **5a**, and also than those of the organic alkynes **9** and **10**, consistent with the contribution of an additional transition within this band in the Ru(II) complexes. The same LC transition (overlapped by the MLCT band at low energy) is also observed for the bis-alkynyl Ru(II) complex **6**, except that its intensity is increased when compared to that of **5b**, in line with the increased number of fluorenyl chromophores present in the alkynyl ligand. The spectrum of the heterobinuclear bis-alkynyl complex **7** also strongly resembles that of **5a**, most probably because the characteristic absorptions originating from the alkynylferrocene ligand, which are often weak in the visible range,[54] remain hidden beneath those of the Ru-alkynyl fragment.[45]

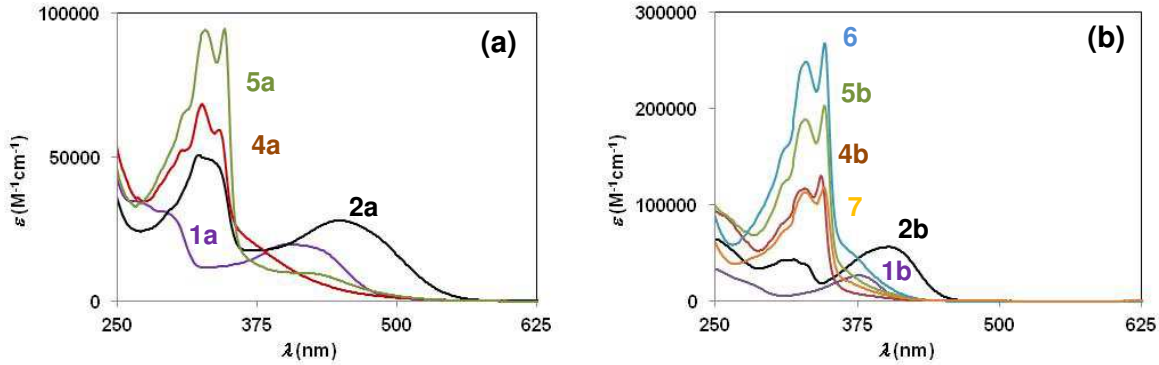

Figure 2. UV-Vis absorption spectra for (a) **1a**, **2a**, **4a** and **5a** and (b) **1b**, **2b**, **4b**, **5b**, **6** and **7** complexes in CH_2Cl_2 at 25 °C.

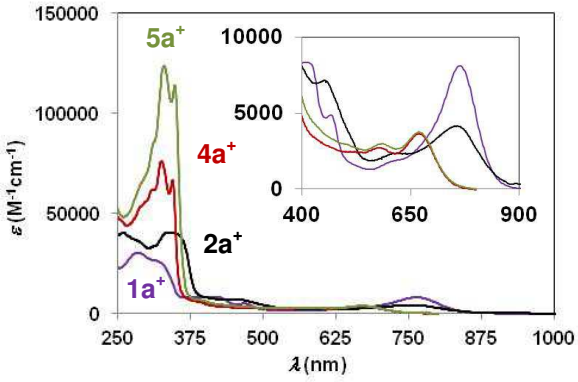

Figure 3. UV-Vis absorption spectra for **1a**[PF_6], **2a**[PF_6], **4a**[PF_6] and **5a**[PF_6] in CH_2Cl_2 at 25 °C.

The UV-Vis-near-IR spectra of the Fe(III) complex cations **2a**[PF_6], **4a**[PF_6] and **5a**[PF_6] were also recorded (Table 2 and Figure 3). The dark blue/green colour of these compounds originates from several overlapping absorptions in the visible range, featuring a maximum on the low energy side in the 650-800 nm range. This first intense absorption, which corresponds to a LMCT transition,[43] occurs at lower energy in the *para*-substituted complex **2a**[PF_6] than in **4a**[PF_6] and **5a**[PF_6], reflecting the energetic ordering observed for the intense fluorene-based LC transitions near 360 nm. A very weak absorption is detected in the near-IR range at ca. 1870 nm, which formally corresponds to a forbidden ligand-field (LF) transition ($d_{Fe}^{1} \leftarrow d_{Fe}^{2}$).[43] The fluorene-based LC transitions observed at 322, 340 and 346 nm for **2a**, **4a** and **5a** undergo bathochromic shifts upon oxidation (to 346, 343 and 347 nm, respectively), which is more pronounced for the *para*-substituted complex **2a**[PF_6].

Spectroelectrochemistry of the Ru(II) Complexes. Due to their greater reactivity, the Ru(III) analogues **2a**[PF_6], **4a**[PF_6], **5a**[PF_6], **6**[PF_6] and **7**[PF_6] were not isolated but instead were generated *in situ* from their Ru(II) parents by spectroelectrochemistry and their electronic spectra recorded (Table 2, Figure 4 and ESI). In contrast to **2b-5b**[PF_6] for which the original spectrum could be restored upon back-reduction to the starting complex **2b-5b**, the oxidation of the bis-alkynyl complexes **6** and **7** was only partially reversible at 25 °C and spectroelectrochemistry had to be performed at lower temperature (-30 °C) to become fully reversible in the chemical sense. The spectrum of these complexes is typical of Ru(III) bis-alkynyl complexes.[55] It reveals that oxidation switches on an intense absorption with a strong LMCT character in the near-IR range. Among the monoalkynyl complexes, this band is more intense and takes place at lower energy for **2a**[PF_6] than for **4a**[PF_6] and **5a**[PF_6]. According to calculations,[37,55] the next transitions at higher energies should be described as $\pi^* \leftarrow \pi$ transitions involving arylalkynyl carbon- and metal-containing MOs.

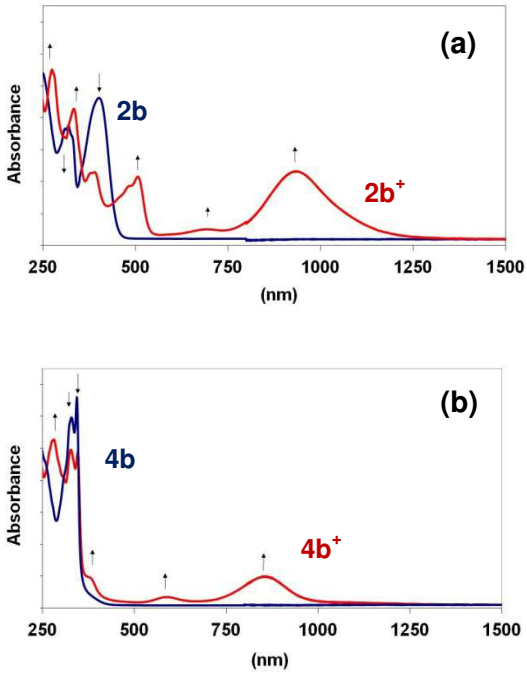

Figure 4. Spectroelectrochemical traces in the near UV-Vis-near-IR range for **2b** (a) and **4b** (b) in CH_2Cl_2 (0.2 M TBAH) at 20 °C.

Excluding the changes in intensity of the LC band near 330 nm and the *ca.* 200 nm (*ca.* 2300 cm^{-1}) bathochromic shift experienced by the first intense absorption in **6**[PF_6], the spectra of the Ru(III) compounds **5b**[PF_6] and **6**[PF_6] (Supporting Information) strongly resemble that of **4b**[PF_6]. In

contrast, the spectroelectrochemistry of **7** deserves some comments (Figure 5). The first oxidation of this complex results in the appearance of two new absorption bands at lower energy than for the neutral parent: one near 570 nm and a second one of nearly similar intensity near 1560 nm, with a shoulder at 2300 nm. The second oxidation results in the disappearance of these absorptions and in the appearance of two new bands at 658 and 1032 nm, which resemble those previously observed for **6**[PF_6] (Supporting Information). These low-energy bands in $\mathbf{7}^{2+}$ can therefore be assigned to ligand-to-metal charge-transfer (LMCT) processes. For $\mathbf{7}^{+}$, the low-energy bands observed at 2300 and 1557 nm more likely correspond to intervalence charge transfer (IVCT) transitions,[56] followed by LMCT transitions at higher energies (569 nm and below).[37,45] This pronounced electrochromism is an important observation for NLO redox-switching purposes, because stepwise oxidation of **7** triggers the appearance of new and specific absorptions in quite distinct spectral ranges.[12] Thus, highly contrasting NLO responses can be anticipated in these specific spectral ranges for each redox state.[55,57]

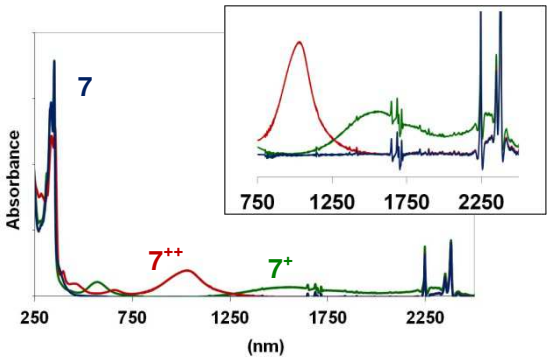

Figure 5. Spectroelectrochemistry in the near UV-Vis-near-IR range for complex **7** in CH_2Cl_2 (0.2 M TBAH) at -30 °C. Inset: expansion of the 750-2500 nm region.

Luminescence Studies. Upon excitation in the 320-380 nm range (corresponding to the LC absorptions) in CH_2Cl_2 solutions at ambient temperatures, all the fluorenyl-containing M(II) and M(III) complexes (M = Fe, Ru) were found to luminesce slightly around 350-370 nm (Figure 6). In line with previous observations made with **1a** and **1b**,[24-25] this luminescence seems to mostly originate from the fluorene-based LC state, rather than from the lowest MLCT state, even when both states overlap such as in the case of **4b-6**. Likewise to **1a** (Table 2), the para-substituted Ru(II) complex **2b** seems also to luminesces weakly ($\Phi_{lum} \leq 0.2$ %) at slightly lower energies (500 nm) when excited at its first MLCT band (Supporting Information). Luminescence from the lowest lying (LMCT and LF) states of the various Fe(III) cations could not be probed due to instrumental limitations.

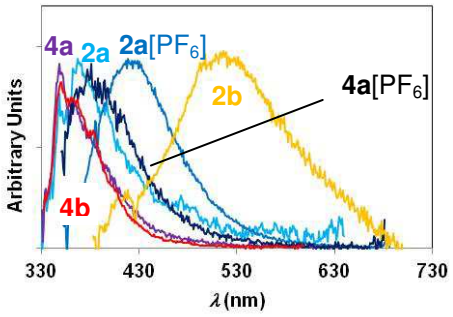

Figure 6. UV-Vis emission spectra for **2a-b**, **4a-b**, **2a**[PF_6] and **4a**[PF_6] complexes in dichloromethane at 300 K.

In all cases, the LC-based fluorescence yields found for the alkynyl complexes are significantly lower than those of their organic alkyne precursors (Supporting information). Thus, the measured yields for the new M(II) and M(III) alkynyl complexes (M = Fe, Ru) are always below 2% (except for **6** or **2b**), whereas yields above 55% were found for all alkyne precursors **8-10** (Supporting Information). Comparing the luminescence yields for the Fe(II) and Ru(II) analogues, it appears that those of the Ru complexes are always superior to those of the Fe complexes. As previously observed, oxidation of the Fe(II) center(s) in **2a**, **4a** and **5a** appears to affect only marginally the emission wavelength of the LC state in the resulting radical cation. However, except for **5a**/**5a**$^+$, oxidation always induces a slight increase in the luminescence quantum yield of these complexes.

Nonlinear Optical Properties. We next determined the cubic hyperpolarizabilities of the new Ru(II) alkynyl complexes **2b**-**5b**, **6** and **7** in solution in CH_2Cl_2 by Z-scan, using femtosecond laser pulses at various incident wavelengths between 550 and 800 nm (Figure 7, Table 3 and Supporting Information).

Consistent with Z-scan measurements on related complexes,[24-25] the nonlinear refraction (γ_{re}) has a negative sign and dominates in absolute value the nonlinear absorption (γ_{im}) at all wavelengths. Focussing on the latter, effective 2PA spectra were obtained for all compounds in the 500-900 nm range (Figure 7). In all nonlinear absorption spectra, there is a strong correlation between $\lambda_{2PA,max}$ and λ_{MLCT} for the first 2PA peak (Table 3), the latter being found at twice the wavelength of the former. This suggests that the transition in the 1PA spectra is the primary origin of the two-photon absorption (2PA) effect. **2b** has an additional 2PA maximum corresponding to twice the wavelength of the second absorption band (ca. 600 nm, which corresponds to a superposition of a second MLCT transition and of the fluorene-centered LC transition). For the meta-linked complexes **4b-6**, this second 2PA band appears at higher energy and its maximum was not always resolved in the spectral range investigated by Z-scan. For all compounds, it is clearly blue-shifted relative to twice the wavelength of the LC band, which is easily identified by its characteristic vibronic structure. This suggests that this 2PA transition does not take place in the LC state but rather in a higher-lying state which is possibly also a MLCT band, analogous to the first 2PA transition of **2b** which is mainly ascribable to population of the first MLCT state.

The cross-section of this first 2PA band is clearly sensitive to the structure of the appended alkynyl ligands. Thus, it decreases in intensity when moving from the para-linked complex **2b** to the meta-linked complex **4b**. This band undergoes a hypsochromic shift that is correlated to the shift of the first MLCT band in the 1PA spectra of these compounds. No further increase (nor shift) is seen when a second fluorenyl group is appended in non-conjugated position to the central phenyl group. As a result, the cross-section of the mono-fluorenyl Ru(II) alkynyl complex **2b** is larger than that of the meta-disubstituted Ru(II) alkynyl complex **5b**, emphazising the importance of π-conjugation between metal centers and 2-fluorenyl units for obtaining large 2PA responses.

Finally, the 2PA cross-section of this first band increases strongly upon progressing from mono- to bis-alkynyl complexes. Thus, the bis-alkynyl complex **6** has the largest cross-section (2270 GM) for the first 2PA peak followed by the heterobinuclear bis-alkynyl complex **7** (1480 GM). Interestingly, the 1PA spectrum of **6** plotted at twice the wavelength does not strongly differ from its 2PA spectrum above 500 nm. However, contrary to what is observed for **7**, the first π^* ← Ru MLCT absorption (shoulder) does not appear to be red-shifted relative to that of **5b**. Given that this complex certainly exists in solution in both co-planar and non-coplanar conformations,[2] observation of its 1PA spectrum resembling that of **5b** and of a single 2PA band similarly shaped to that of **5b** indicates that all conformers of **6** absorb at fairly similar energies. Indeed, the centrosymmetric nature of complex **6** in its coplanar conformation forbids 1PA and 2PA to take place in similar excited states (exclusion rule), so non-coplanar conformations with non-forbidden 2PA must be strong contributors in solution.

Table 3. Nonlinear Optical Data at Wavelengths of the Apparent 2PA Extrema in CH_2Cl_2 (unless otherwise indicated).

	λ_{1PA} [a] (nm)	λ_{2PA} [b] (nm)	γ_{re} (10^{-34} esu)	γ_{im} (10^{-34} esu)	$\lvert\gamma\rvert$ (10^{-34} esu)	σ_2 [c] (GM)	Ref
1a [d]	404	740	-25 ± 15	14 ± 2	28 ± 15	330 ± 50	[24]
1a [e]	404	740	-160 ± 17	84 ± 16	180 ± 25	2400 ± 470	[24]
1b	373	720	–15 ± 5	12 ± 2	19 ± 5	360 ± 60	[25]
1a$^+$	764	760	-99 ± 10	-11 ± 2	100 ± 10	-300 ± 45	[24]
2a	448	760	-87 ± 9	14 ± 2	88 ± 9	370 ± 60	[24]
2a$^+$	756	760	-1200 ± 32	-250 ± 76	1200 ± 330	-6700 ± 2100	[24]
2b	308	600	-136 ± 26	22 ± 7	138 ± 27	990 ± 340	this work
	401	800	-39 ± 5	44 ± 8	59 ± 9	1075 ± 190	
3	489	1000	–35 ± 70	55 ± 19	66 ± 73	860 ± 290	[25]
4b	343	700	87 ± 20	21 ±5	90 ±21	920 ± 170	this work
5b	≈365	700	-22 ± 6	30 ± 3	38 ± 7	950 ± 110	this work
6	≈364	720	-71 ± 25	76 ± 14	104 ± 28	2270 ± 410	this work
7	≈372	700	-31 ± 9	47 ± 5	56 ±11	1480 ± 170	this work

[a] Maximum of the first 1PA (MLCT) band. [b] Maximum of the first 2PA band. [c] Apparent 2PA cross-section of the 2PA band. [d] Determined in THF. [e] Suspected to undergo a photochemical reaction in CH_2Cl_2 contributing to an increase in the apparent 2PA cross-section measured by Z-scan.[24]

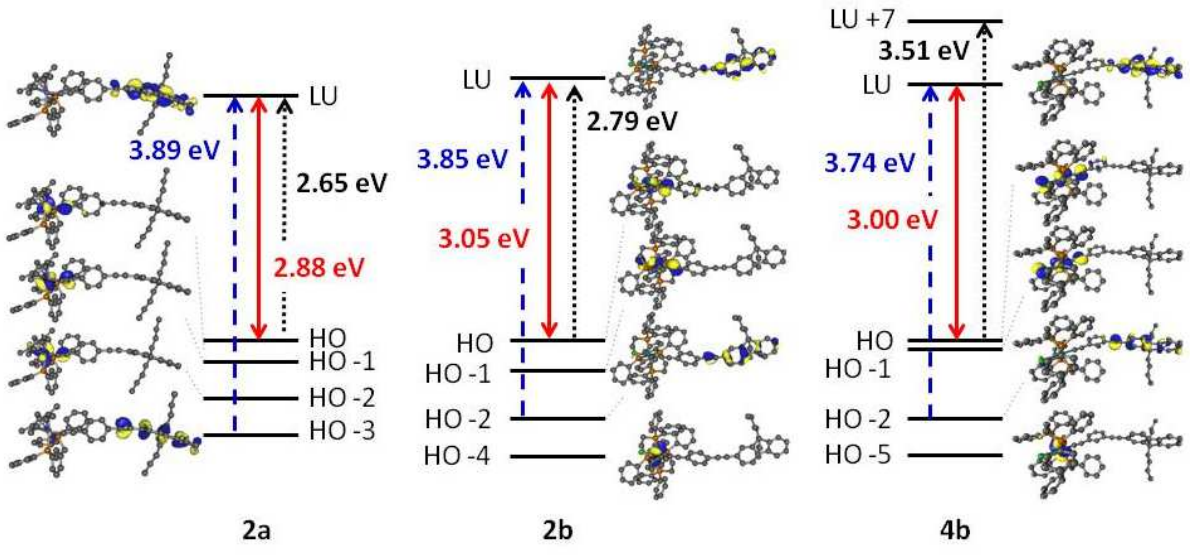

Figure 8. Selected metallic and fluorenyl-based Kohn-Sham frontier molecular orbitals for **2a**, **2b** and **4b** illustrating the HOMO-LUMO gap (red arrows). The first MLCT and LC transitions with significant oscillator strength (TD-DFT, see Supporting Information, Tables S7-S9) are indicated by dark arrows and dashed blue arrows, respectively. Hydrogen atoms are omitted for clarity.

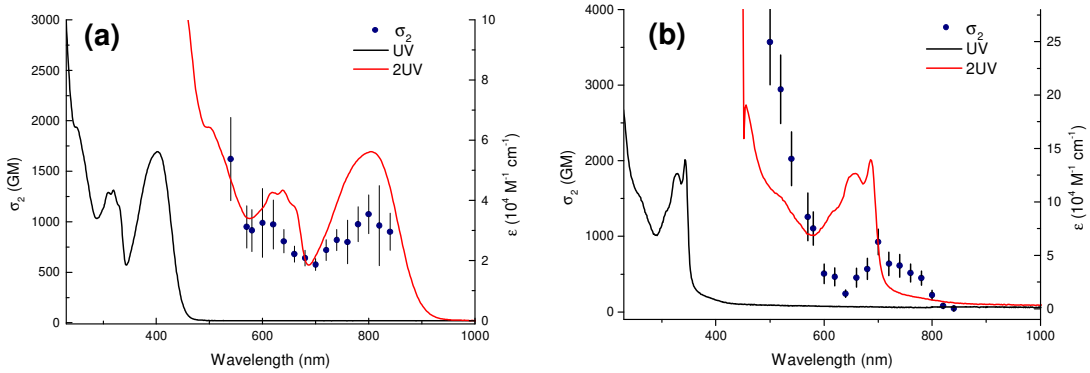

Figure 7. Apparent two-photon absorption cross-sections (in Göppert-Mayer units) for **2b** (a) and **4b** (b) in dichloromethane at 25 °C by open-aperture Z-scan measurements. The 2PA spectral data are overlaid by the one-photon absorption spectrum (black) and the one-photon absorption spectrum plotted at 2λ (red).

DFT Calculations. Ground state optimizations have been performed on **2a**, **2b** and **4b** at the DFT/B3LYP*-D3/def2-TZVP(-f) level of theory with ZORA scalar relativity (Supporting Information). These calculations reveal that ruthenium complexes **2b** and **4b** have their HOMO and HOMO-1 localized on the Cl–Ru–C≡C endgroup while their HOMO-2 is fluorenyl-based (Figure 8). For the iron complex **2a**, as previously shown,[24] the three highest-energy occupied orbitals (HOMO, HOMO-1 and HOMO-2) are localized on the Fe–C≡C organoiron fragment,while the fourth one (HOMO-3) is on the fluorenyl fragment group. In contrast, for the ruthenium complexes **2-4b**, a deeper lying one (HOMO-4 or HOMO-5, resp.) is again centered on ruthenium. Thus, the assignment of the first oxidation step as mostly metal-localized is appropriate for all M(II) complexes. In all three cases, the LUMO is localized on the fluorenyl fragment.

The lowest triplet and quintet excited states were then optimized for **2a** by unrestricted DFT, as well as the the lowest triplet excited state for **2b**. In the case of **2a**, singlet/triplet, triplet/quintet and singlet/quintet minimum energy crossing points (MECPs) were also optimized (see Computational Details and Supporting Information for selected geometrical parameters), permitting us to propose a more complete picture of the possible nonradiative deactivation processes for this particular compound (Figure 9). This study revealed that all lowest-lying excited states are of metal-centered character for M(II) complexes (see the singly-occupied natural orbitals in the Supporting Information). According to our calculations, intersystem crossing to low-lying triplet (and quintet) LF states affords a likely decay pathway for both families of M(II) compounds, regardless of the nature of the metal center. As shown for complex **2a**, population of the ^{3}LF or ^{5}LF states is thermodynamically favored. Either of these excited states can easily deactivate nonradiatively via intersystem crossing to the ground state (GS) through highly accessible MECPs. In this scheme, the distortion coordinate combines contributions from Fe–P, Fe–Cp* and to a lesser extent Fe–alkynyl bond elongations (Supporting Information). The principal differences between the Fe(II) and Ru(II) complexes resides in the energetic gap between the GS and the first ^{3}LF triplet state which is roughly 1 eV larger for Ru(II) complexes (**2a**: 0.95 eV; **2b**: 2.21 eV and **4b**: 2.27 eV). Furthermore, TD-DFT calculations (Supporting Information, Tables S7-S9) reveal that for the para complexes **2a-b**, the (forbidden) transition to the first singlet ^{1}LF states (**2a**: 3.80 eV; **2b**: 3.78 eV) takes place at slightly lower energies than those to the first ^{1}LC states (**2a**: 3.89 eV; **2b**: 3.85 eV), providing additional potential decay pathways when these LC states are populated. For the meta complex **4b**, however, this first ^{1}LF states is not found among the first 40 computed states, its energy being therefore slightly higher.

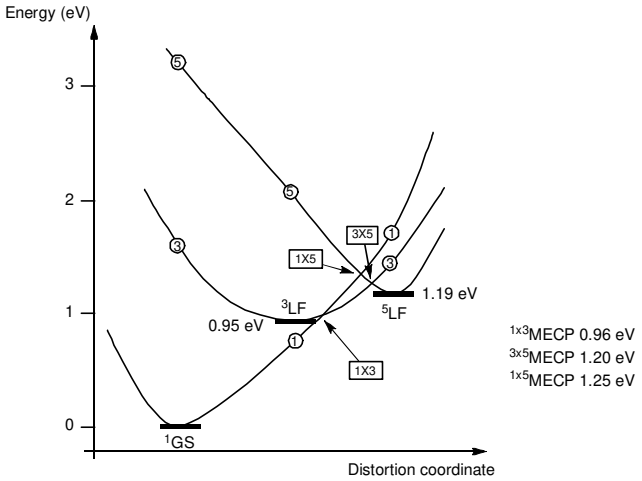

Figure 9. Schematic potential energy curves for complex **2a**, showing low-lying LF excited states (^{3}LF and ^{5}LF) and minimum energy crossing points (MECPs) that are involved in the proposed relaxation pathways to the GS. For comparison purposes, the potentially emitting states (not shown) are found around 3 eV (^{1}MLCT) and 4 eV (^{1}LC) by TD-DFT at the GS geometry. Thick bars are global minima. Numbers in circles correspond to single point energy calculations. Rectangular boxes depict MECPs.

DISCUSSION

A new set of metal alkynyl complexes has been synthesized and the linear and nonlinear optical properties of selected examples have been investigated in their M(II) and M(III) redox states (M = Fe, Ru). Along with the data previously gathered on closely related complexes (**1a-b**, **2a**, **3**),[24-25] several conclusions can be drawn regarding their linear and third-order nonlinear optical properties.

Redox-Dependent Electronic Absorption. In line with previous DFT calculations,[24] a reduction in the HOMO-LUMO gap is evidenced in each case, upon proceeding from the 2-fluorenylethynyl complexes (**1a-b**) to those possessing corresponding alkynyl ligands extended with a phenylethynyl unit (**2a-b**, **4a-b**). This structural modification translates into the appearance in their absorption spectra of an MLCT transition possessing a marked fluorenyl character at a lower energy than for **1a-b**. This first MLCT transition occurs at a lower energy for the para-substituted complexes (**2a-b**) than for their meta-substituted analogues **4a-b**. In the latter complexes, it also overlaps with the fluorene-centered $\pi^*\leftarrow\pi$ (LC) excitation, easily recognizable by its vibronic fine structure. For the larger meta-substituted homologues **5a-b**, qualitatively similar absorptions are observed as for **4a-b**, although two 2-fluorenylethynyl ligands are now appended to the phenylene linker. The increase in the number of fluorenyl groups translates into a relative increase in the intensity of the LC band. Similar spectral features are seen for the bis-alkynyl Ru(II) complexes **6** and **7**.

Upon mono-oxidation the corresponding M(III) radical cations are formed. Depending on whether Fe(II) or Ru(II) complexes are oxidized, mono-oxidation occurs at similar potentials for each type of complex (-0.12 ± 0.02 V or 0.60 ± 0.05 V, respectively), the Ru(III) cations being much more reactive than their Fe(III) analogues in solution. For these radical cations, the first MLCT band is shifted to higher energy, while new LMCT bands of moderate intensity appear at the visible/near-IR edge (680-760 nm for Fe(III) or 850-1100 nm for Ru(III)) along with very weak (formally forbidden) LF bands in the near-IR/IR range (observed around 1850 nm in the case of the Fe(III) complexes). Thus, all these fluorenylalkynyl complexes exhibit a strong linear electrochromism resulting in a pronounced colour change from red/orange to deep-green/deep-blue in solution. As previously discussed,[24] this

electrochromism can be usefully exploited to reversibly switch their linear or nonlinear optical properties in a spectroelectrochemical cell,[12,19,55] provided water and oxygen are carefully excluded from the electrolytic solution.[58]

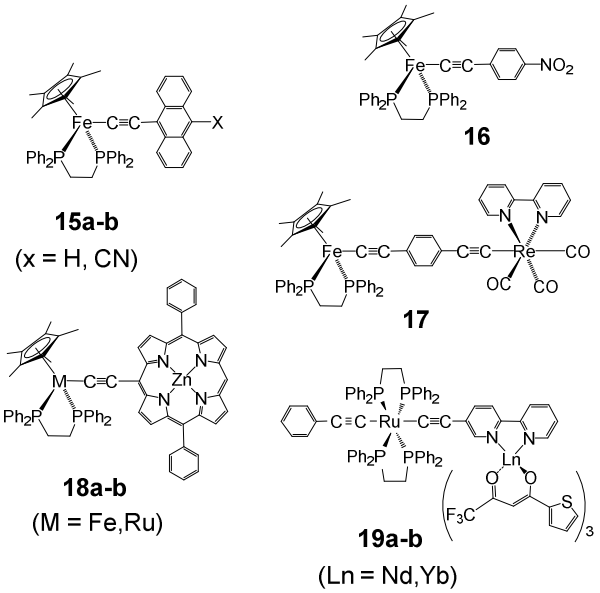

Chart 4. Selected Examples of Redox-switchable Lumino-phores.

Luminescence. As exemplified by the data gathered on **8-10**, the 2-ethynylfluorenyl-containing arylalkynyl ligands are usually powerful organic luminophores.[59] However, when functionalized by the organometallic [Fe(η^5-C_5Me_5)(κ^2-dppe)]$^{n+}$ or *trans*-[Ru(κ^2-dppe)$_2$Cl]$^{n+}$ end groups, efficient quenching of the ligand-based luminescence takes place, regardless of the oxidation state (n = 0, 1). As previously underlined by us and others,[10,24-25] the weak luminescence detected for all these complexes does usually not originate from the lowest-lying excited state, but most likely from a higher lying luminophore-based LC state, in violation of Kasha's rule.[60] This constitutes a rather unusual phenomenon,[61] but one which has precedence with organometallic chromophores,[62] including the closely related complexes **15a-b**$^{n+}$ (n = 0, 1),[10] **16**,[63] **17**$^{+}$,[11] and **18a-b**$^{+}$,[9] (Chart 4).[64]

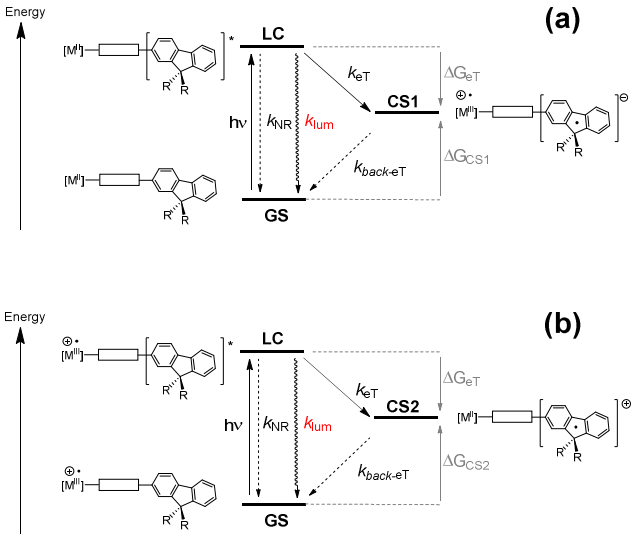

Scheme 5. LC-Based Luminescence Trapping Process of a M(II) (a) or M(III) (b) Complex.

When M(II) (or M(III)) complexes are excited in the fluorene-based band, our redox study in combination with the use of Rehm-Weller equations (eqs 4-5) reveals that the corresponding charge-separated state CS1 (or CS2) can be formed via a photo-induced intramolecular electron-transfer mechanism, given the positive driving force (ΔG_{eT}) found in each case for this process. The latter state most likely corresponds to the first MLCT (or LMCT) excited state of the complex (Scheme 5). Based on the Marcus-Hush treatment,[33,65] estimates of the corresponding activation barriers ($\Delta G^{\neq}$) were derived for this electron quenching process (eq 3), in addition to its rate (k_{eT}; eq 2). However, no clear correlation between these data and the experimentally measured luminescence quantum yields was found for compounds with comparable electronic couplings (H_{ab}) such as **1a-b**/**1a**$^+$, **2a-b**/**2a**$^+$ or **4-6**/**4a**$^+$ (Supporting Information), nor between all compounds when corrections for the different H_{ab} are considered; this suggests that a redox-quenching process does not dominate the nonradiative decay of the LC state. This is unsurprising given that deactivation of this state into the lower-lying MLCT (or LMCT) state can also take place via other processes (Scheme 6a). Thus, conversion of this LC state into other lower-lying (dark) singlet or triplet ligand field (LF) states (see below) via nonradiative processes (internal conversion or intersystem crossing) will also contribute to its decay in a competitive way. As a result, any structural modification (Fe vs. Ru exchange or meta vs. para bonding) effected on these compounds to modify the driving force for the redox quenching process has only a marginal effect on the LC-based luminescence of these compounds. Thus, in line with previous results,[25] the luminescence quantum yields measured for this LC-based emission are definitively not controlled by the redox trapping reaction forming the lower-lying CT state.

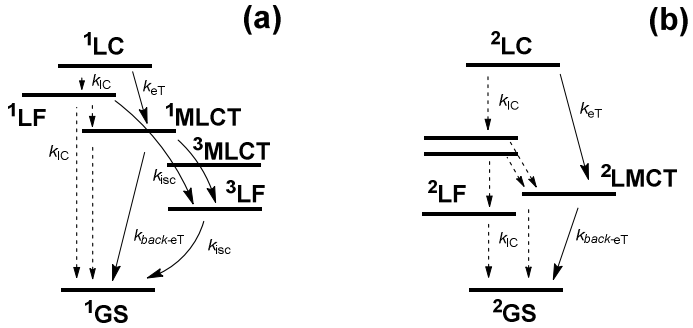

Scheme 6. Some nonradiative deactivation pathways operative for (a) M(II) and (b) M(III) complexes (IC: internal conversion, (back-)eT: (back-)electron-transfer; isc: intersystem crossing).

The lower-lying excited CT or LF states possess very efficient nonradiative decay channels, resulting in nearly total quenching of the luminescence for most of the M(II) (or M(III)) complexes. In line with previous reports,[10,24-25] we could not detect any luminescence originating from the first MLCT state of most of the new M(II) complexes investigated. Thus, along with **1a-b**,[24-25] only in the case of the Ru(II) complex **2b** could a very weak emission from the MLCT state be determined, as expected for a class of compounds known to be luminescence quenchers.[66] In several instances, selected bis-alkynyl complexes have been shown to be emissive from their first excited state. However, in these cases, either the MLCT character of the emissive state is totally absent, as in **19a-b**,[8] or it is strongly admixed with another character (such as LLCT, for instance).[5] The rapid nonradiative deactivation of the first MLCT state of the Fe(II) alkynyl complex **16** has previously been investigated by ultrafast transient absorption.[63] In addition to the expected back-electron transfer to the GS, other pathways involving intersystem crossing to lower-lying (dark) triplet ligand field (LF) states have been evidenced. In line with this former study, DFT calculations confirm the existence of low lying triplet ligand-field (^{3}LF) states for the fluorenyl-alkynyl M(II) complexes (around 1 eV for Fe(II) and 2.3 eV for Ru(II)) and clearly show the potential relevance of the latter state for nonradiative relaxation. Thus, besides back-electron transfer, intersystem crossing to ^{3}LF states (and possibly to ^{5}LF states for Fe(II) complexes) can also regenerate the GS in a non-radiative way. Similar to **19a-b**,[8] more luminescent M(II) alkynyl

complexes can however be obtained when the emitting state is at sufficiently low energy to avoid efficient quenching by ^{1}MLCT and ^{3}LF states. Such a situation was never reached with the alkynyl compounds in the present study, but it was approached with the Ru(II) complex **6**, which, as a result, possesses the highest luminescence yield.

Regarding the M(III) complexes, their first excited states correspond to ^{2}LF states. However, such ^{2}LF states were experimentally detected by electronic absorption only in the case of the Fe(III) mono-alkynyl complexes,[43] not in the case of mono-alkynyl Ru(III) complexes.[37,41] In the latter case, only the first ^{2}LMCT state in the near-IR range is usually observed. Based on the energy gap law,[67] these low-lying states should be essentially non-luminescent and, to our knowledge, their luminescence has never been probed. In the present case, it is the luminescence of the ^{2}LC (fluorenyl-based, but the unpaired spin is localized on the M(III) center) state at higher energies (around 330 nm) that was detected. Considering the larger activation energies derived for the redox trapping process (see Supporting Information), nonradiative deactivation via the CS2 state appears less likely than for their M(II) parents (via the CS1 state). This possibly partly explains the increased luminescence quantum yields found for most of the Fe(III) compounds compared to their Fe(II) parents. However, here again, the presence of several excited states in between their first excited states and the emissive ^{2}LC states opens many channels for nonradiative deactivation other than electron-transfer pathways, explaining why the increase in quantum yield does not inversely correlate with k_{eT}. Thus, efficient non-radiative deactivation takes place in both M(II) and M(III) redox states.[68] Consistent with previous examples, such as **15a-b** $^{n+}$,[10], **17**$^{n+}$,[11] or **18a-b**$^{n+}$,[9] the present investigation with **1a**$^{n+}$, **2a** $^{n+}$ and **4a** $^{n+}$ (n = 0, 1) reveals a poor luminescence quantum yield for the most luminescent Fe(III) parent along with a modest contrast in quantum yield with the other redox parent.

Cubic NLO Properties. As often observed for d^6-metal alkynyl complexes,[16-17] the real part of the cubic molecular polarizability is negative in the visible range and dominates the modulus of γ (Supporting Information). The imaginary part (γ_{im}) is usually positive for M(II) complexes and gives rise to "effective" two-photon absorption peaks at wavelengths that coincide with twice their wavelength of 1PA peaks.[24-25] In this respect, the new nonlinear absorption measurements on the Ru(II) complexes are far less noisy that the data previously gathered on corresponding Fe(II) alkynyl complexes, which were also much more air-sensitive and prone to undergo photoreactions in the solvent. Based on the new data obtained for the Ru(II) compounds, we can now better analyse the influence of structural changes on the lowest energy 2PA peaks, an important issue given the increasing societal implications of two-photon absorption.[28,69]

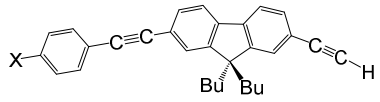

20a-c
(X = NPh_2, NH_2,OMe)

Chart 5. Examples of Fluorene-containing Organic Two-photon Absorbers.

First of all, and consistent with previous work on these compounds,[24] we show here that metallated alkynes such as **2a-b** or **4a-b** are much better two-photon absorbers than purely organic derivatives of similar structure such as **20a-c** (Chart 5), for which much lower 2PA cross-sections have been reported (between 15-80 GM for their lowest energy 2PA peaks).[59] Definitive information about the influence of the nature of the organometallic center for similar alkynyl ligands cannot be gained from

comparison between the data available for **1-2a** and **1-2b** in CH_2Cl_2, given the photostability problems of the organoiron complexes **1-2a** in this solvent. Based on the available measurements made for **1a** and **2b** in THF,[24] slightly more pronounced global nonlinear responses (due to nonlinear refraction) are seen for [Fe(η^2-C_5Me_5)(κ^2-dppe)] complexes compared to their *trans*-[Ru(κ^2-dppe)$_2$Cl] analogues, while higher apparent 2PA cross-sections are found for the Ru(II) examples. Furthermore, whereas the wavelength of the first 2PA peak is nearly coincident with twice the wavelength of the first MLCT excited state peak for the latter complexes, a sizeable blue-shift between these data is observed for the Fe(II) analogues. Such a shift indicates that either (i) a slightly more energetic electronic state that overlaps with the first MLCT 1PA band or (ii) higher vibronic substates of the first MLCT state[70] are populated by two-photon absorption with the Fe(II) complexes. Overlooking the existence of this shift, we have previously considered that the first 2PA peak did correspond to a transition taking place in the fluorenyl-based LC state instead of the MLCT state for **1a-b**.[24] In the light of the new data obtained for **2b**, **4b**, **5b** and **7** and that previously obtained for their analogues **1b** and **3** (Chart 1),[25] we are now inclined to consider that the first 2PA peak corresponds to a transition taking place in the first MLCT state, the 2PA maximum being blue shifted relative to the corresponding 1PA peak for Fe(II) complexes; the metal character seems important for boosting 2PA, consistent with independent reports.[71]

Comparison of the data obtained for the new mono-alkynyl Ru(II) complexes **2b**, **4b** and **5b** with those previously obtained for the Ru(II) complex **1b**[25] indicates a clear increase in the 2PA response upon extension of the π-manifold of the alkynyl ligand, regardless of the connectivity considered (**2b** or **4b**). Thus, the following trends emerge from our data: (i) a gradual increase of the first 2PA peak takes place with the increasing size of the conjugated π-manifold of the alkynyl ligand (i.e. when progressing from **1b** to **2b**); (ii) this increase occurs at the expense of some transparency in the visible range; (iii) increasing the number of 2-fluorenyl units in the alkynyl ligand in non-conjugated positions does not significantly improve the magnitude of the 2PA peak (i.e. when progressing from **4b** to **5b**); (iv) progressing from a purely dipolar mono-alkynyl structure such as **5b** to the centrosymmetric *trans*-bisalkynyl structure **6** results in more than doubling the 2PA without reduction of the transparency window; (v) replacement of the *trans*-chloride ligand in **4b** by a ferrocenylethynyl ligand in **7** improves the cross-section of the first 2PA peak, while opening additional opportunities for redox-control of linear and nonlinear absorption (Figure 5). The merits of the ethynylferrocene-capped bis-alkynyls have been assessed in previous reports and shown to roughly double the cross-section when compared to mono-alkynyl analogues;[16,72] the present data are consistent with this. With respect to our previous contribution,[25] DFT calculations with **1-4b** indicate that the structural changes leading to augmentation of the 2PA activity induce a bathochromic shift in the first MLCT transition, which does not always correlate to the HOMO-LUMO gap of the complexes (Figure 8). While published data for related complexes indicate that *trans*-bis(alkynyl) Ru(II) derivatives are usually more 2PA-active than their chloro-mono(alkynyl) Ru(II) counterparts,[16,72] for **6** the corresponding improvement over **5b** cannot be solely attributed to a reduction of the HOMO-LUMO gap or to a MLCT state at lower energy (compare the data obtained for the bis-alkynyl complexes **3** and **7**). This improvement partly originates from the symmetry change, **6** possessing a quadrupolar structure with an inversion center (in its planar conformation) instead of a dipolar (**1-4b**) or dissymmetric multipolar structure (**3**,**7**).[28,34] Similar statements have also been previously made for organoiron alkynyl complexes.[24]

As regards redox-control of the NLO activity, the qualitatively similar linear electrochromism evidenced for all these alkynyl complexes makes them likely to behave as nonlinear electrochromes at the visible-near-IR edge. As previously evidenced with **1a** and **2a**,[24] the good spectral overlap of their first 2PA band of **4a** and **5a** with the LMCT band of their Fe(III) parents near 700 nm is perfectly suited to impart dramatic redox-induced changes to their third-order NLO response in this spectral range.[12,55] More elaborate (multi-state) switching schemes might equally be observed for **7** in the same spectral range.

CONCLUSION

We have reported here the synthesis and characterization of a new set of redox-active iron and ruthenium phenylalkynyl complexes featuring 2-fluorenyl extensions. The linear and third-order nonlinear optical properties of these organometallic complexes were studied by spectroelectrochemistry, fluorimetry and Z-scan in their neutral and stable cationic redox states.

First, we have shown that these compounds possess very strong linear electrochromism in the visible range with oxidation reducing dramatically their transparency window, due to the appearance of LMCT and LF absorptions in the near-IR/IR range. This oxidation takes place at lower potentials for the Fe(II) compounds. The Fe(III) parents are therefore far less reactive in solution than their Ru(III) counterparts. As a result, Fe(II) complexes are better suited for repetitive redox switching (under inert atmospheres).[19] In contrast, the Ru(II) analogues, which also possess the larger transparency windows, are ideal NLO-phores for aerobic uses in their neutral state.

Then we have shown that molecular engineering of the alkynyl ligand aimed at slowing down through-ligand electron transfer hardly impacts their luminescence. Regardless of the nature of the metal centre (Fe or Ru) and of its oxidation state, very weakly luminescent complexes are always found. With the help of excited-state theoretical calculations, we have shown that several competitive deactivation mechanisms likely contribute to the non-radiative decay of the photoexcited state(s), in particular via the LF manifold, explaining the poor redox-dependence of luminescence for this class of compounds.

Finally, and more importantly, we have shown that the Ru(II) alkynyl complexes exhibit significant NLO responses in the near-IR domain (with dominant negative nonlinear refraction). Interestingly, a large 2PA activity in the 600-800 nm range was also evidenced for these compounds and useful structure-property relationships were determined. Thus, by extending the size of the conjugated π-manifold on the alkynyl ligand, a clear increase in the 2PA response takes place, emphasizing the importance of para- vs. meta- connection of 2-fluorenylethynyl groups on the phenylethynyl spacer. Concomitantly, 2PA is also shifted to slightly lower energies. Upon progressing from mono- (dipolar) to bis-alkynyl (quadrupolar) complexes, a further increase in the 2PA cross-section can be obtained. Furthermore, considering the marked linear electrochromism stated for these complexes, a significant nonlinear electrochromism is also expected in the near-IR range depending on the incident wavelength. This remarkable property will be the subject of future investigations.

EXPERIMENTAL SECTION

General Data. All manipulations were carried out under an inert atmosphere of argon (Fe complexes) or dry nitrogen (Ru complexes).[73] Solvents and reagents were used as follows: MeOH, distilled from MgOMe; THF, Et_2O and *n*-pentane, distilled from Na/benzophenone; CH_2Cl_2, distilled from CaH_2, purged with Ar, and opened/stored under Ar. High field NMR spectra experiments were performed on multinuclear Bruker 500 MHz, 300 MHz or 200 MHz instruments. Chemical shifts are given in parts per million (ppm) relative to tetramethylsilane (TMS) for ^{1}H and ^{13}C NMR spectra and external H_3PO_4 for ^{31}P NMR spectra. Experimental details regarding measurements on paramagnetic Fe(III) complexes can be found in previous contributions.[44,74] Transmittance-FTIR spectra were recorded using a Bruker IFS28 or Perkin-Elmer System 2000 spectrometers (400-4000 cm^{-1}). Raman spectra of the solid samples were obtained by diffuse scattering on a LabRAM HR 800 Raman micro-spectrometer

equipped with a confocal microscope and recorded in the 800-2500 cm^{-1} range (Stokes emission) with a laser excitation source at 785 nm (25 mW). Cyclic voltammograms were recorded with an e-corder 401 potentiostat system from eDaq Pty Ltd. by using a Pt disk as working electrode, a Pt wire as counter electrode and an Ag/AgCl or a SCE reference electrode while spectroelectrochemical experiments were performed using a homemade OTTLE cell, as described below. For the more anodic or cathodic scans another homemade setup made of a Pt disk electrode (diameter 1 mm), a vitreous carbon rod as counter electrode and as reference electrode. The latter was either (i) a silver wire in a 0.1 M $AgNO_3$ solution in CH_3CN for the anodic studies or (ii) a Ag/AgI, I^- in 0.1 M NBu_4I solution in DMF for the cathodic studies. This three electrode cell was connected to a PAR Model 273 potentiostat/galvanostat (PAR, EG&G, USA) monitored with the ECHEM Software. Activated Al_2O_3 was added in the electrolytic solution to remove excess moisture. The $FeCp_2^{0/1+}$couple (ΔE_p = 0.09 V; i_{pa}/i_{pc} = 1) was used each time as an internal calibrant.[75] UV-Visible spectra were recorded using a Cary 5000 spectrometer in the 200-2500 nm range and are reported as λ_{max} (nm) [ε (10^3 M^{-1} cm^{-1})]. Fluorescence spectra were recorded using a FLS 920 Edinburgh Instrument spectrofluorimeter. HRMS and elemental analyses were performed at CRMPO or at the Research School of Chemistry, Australian National University. Flash column chromatography[76] was performed using silica (Scharlau 60, 230-400 mesh) or basic alumina (Aldrich, Brockman activity I, ca. 150 mesh); 3% Et_3N was added to the eluent for column chromatography of ruthenium complexes. The size of the column is given as (height) × (diameter) in cm.

Unless specified, all reagents were of commercial grade. 3,5-Dibromobenzaldehyde,[77] 9,9-dibutyl-2-bromofluorene (**5**),[24] and LiN^iPr_2 (LDA)[78] solutions in THF were prepared as described in the literature and *n*-BuLi was titrated with diphenylacetic acid before use.[79] The syntheses of the organic alkyne precursors **8**, **9** and **10** are given in the Supporting Information. Compound **8** was previously synthesized via another synthetic approach.[24] Fe(η^5-C_5Me_5)(κ^2-dppe)Cl,[80] [Ru(κ^2-dppe)$_2$(Cl)][PF_6][81] and ethynyl-ferrocene[82] were prepared according to published procedures.

Synthesis of the Fe(II) Alkynyl Complexes

General Procedure. The organic alkyne (0.55 mmol), KPF_6 (0.55 mmol) and the iron precursor Fe(η^5-C_5Me_5)(κ^2-dppe)Cl (0.44 mmol) were dissolved in a mixture of THF (10 mL) and MeOH (10 mL) and stirred 12 h at room temperature. The reaction mixture was evaporated in vacuo and extracted with CH_2Cl_2 (3 × 10 mL) via a filter paper-tipped cannula. The resulting brown solution was concentrated to ca. 2 mL and the vinylidene salt was precipitated by addition of *n*-pentane. The precipitate was washed with *n*-pentane (20 mL) and dried under vacuum, providing the desired vinylidene complex as a brown-orange powder (65-70% yield; see Supporting Information). This vinylidene complex (0.15 mmol) was then dissolved in THF (20 mL) and *t*-BuOK (1.00 mmol) was added. The dark red reaction mixture was stirred for 15 min. Solvents and volatiles were evaporated under vacuum. The reaction mixture was then extracted with toluene (3 × 20 mL) and passed through Celite® (2 × 2 cm). The resulting dark red solution was concentrated to dryness, CH_2Cl_2 (2 mL) was added, and the desired complex was precipitated by addition of MeOH at 0 °C. The precipitate was then washed with MeOH (2 × 10 mL) at 0 °C and dried in vacuo, providing the corresponding alkynyl complex as an orange to orange-red powder.

Fe(η^5-C_5Me_5)(κ^2-dppe){C≡C(1,4-C_6H_4)C≡C(2-$C_{13}H_7Bu_2$)} (2a). From 325 mg of **2a-v**[PF_6] and 118 mg of *t*-BuOK, 220 mg of **2a** were isolated (76%).[24]

Fe(η^5-C_5Me_5)(κ^2-dppe){C≡C(1,3-C_6H_4)C≡C(3-$C_{13}H_7Bu_2$)} (4a). From 350 mg of **4a-v**[PF_6] and 112 mg of *t*-BuOK, 200 mg of **4a** were isolated (71%). Anal. Calc for $C_{67}H_{68}FeP_2$•MeOH: C, 79.83%; H, 7.09%;

found: C, 79.91 %; H, 6.77%. MS (ESI) m/z calc. for $C_{67}H_{68}FeP_2$ [$M^{+\bullet}$]: 990.4146; found: 990.4143. IR (KBr, cm^{-1}): $\bar{\upsilon}$ = 2202 (w, C≡C); 2042 (s, Fe-C≡C). Raman (neat, cm^{-1}): $\bar{\upsilon}$ = 2199 (m, C≡C); 2036 (s, Fe-C≡C). $^{31}P\{^1H\}$ NMR (121 MHz, C_6D_6): δ = 100.1 (s, P_{dppe}). ^1H NMR (300 MHz, C_6D_6): δ = 7.98 (m, 4H, H_{Ar}), 7.68 (d, $^3J_{H,H}$ = 8.8 Hz, 2H, H_{Ar}),7.59-7.03 (m, 25H, H_{Ar}), 2.62 (m, 2H, $CH_{2/dppe}$), 1.89 (t, $^3J_{H,H}$ = 8.2 Hz, 4H, $CH_{2/Bu}$), 1.81 (m, 2H, $CH_{2/dppe}$), 1.51 (s, 15H, C_5Me_5), 1.02 (m, 4H, $CH_{2/Bu}$), 0.75-0.56 (m, 10H, $CH_{2/Bu}$ + $CH_{3/Bu}$). $^{13}C\{^1H\}$ NMR (75 MHz, C_6D_6): □ = 151.4 & 151.1 (2×s, C_{Flu}), 141.5 & 141.2 (2×s, C_{Flu}), 141.3 (t, $^2J_{C,P}$ = 39 Hz, Fe*C*≡C), 139.7 & 137.8 (m, $C_{Ar/dppe}$), 134.5 (m, $CH_{Ar/dppe}$), 133.8, 131.9, 131.3, 130.6 (4s, CH_{Ar}/C_{Ar}), 129.3 & 129.1 (2×s, $CH_{Ar/dppe}$), 128.6-127.5 (m, CH_{Ar}/C_{Ar}/ $CH_{Ar/dppe}$), 126.4, 126.2, 123.8, 123.1, 120.5, 120.2 (6×s, CH_{Ar}/C_{Ar}), 119.9 (s, FeC≡*C*), 91.5 & 90.3 (2×s, C≡C), 88.0 (s, $C_5(CH_3)_5$), 55.4 (s, C_{Flu}), 40.6 (s, $CH_{2/Bu}$), 31.1 (m, $CH_{2/dppe}$), 26.4 (s, $CH_{2/Bu}$), 23.5 (s, $CH_{2/Bu}$), 14.0 (s, $CH_{3/Bu}$), 10.3 (s, $C_5(CH_3)_5$).

Fe(η^5-C_5Me_5)(κ^2-dppe){C≡C(1,3,5-C_6H_3)[C≡C(2-$C_{13}H_7$-Bu_2)]$_2$} (5a). From 490 mg of **5a-v**[PF_6] and 112 mg of *t*-BuOK, 330 mg of **5a** were isolated (75%). Anal. Calc for $C_{90}H_{92}FeP_2$•MeOH: C, 82.58%; H, 7.31%; found: C, 82.38%; H, 7.13%. MS (ESI) m/z calc. for $C_{90}H_{92}FeP_2$ [$M^{+\bullet}$]: 1290.6024; found: 1290.6017. IR (KBr, cm^{-1}): $\bar{\upsilon}$ = 2207 (w, C≡C); 2043 (s, Fe-C≡C). Raman (neat, cm^{-1}): $\bar{\upsilon}$ = 2204 (m, C≡C); 2044 (m, Fe-C≡C). $^{31}P\{^1H\}$ NMR (121 MHz, C_6D_6): δ = 100.2 (s, P_{dppe}). ^1H NMR (300 MHz, C_6D_6): □ = 7.99 (m, 4H, H_{Ar}), 7.75 (s, 1H, H_{Ar}), 7.69 (s, 2H, H_{Ar}), 7.55-7.06 (m, 30H, H_{Ar}), 2.61 (m, 2H, $CH_{2/dppe}$), 1.83 (t, $^3J_{H,H}$ = 8.1 Hz, 8H, $CH_{2/Bu}$), 1.81 (m, 2H, $CH_{2/dppe}$), 1.51 (s, 15H, C_5Me_5), 1.04 (m, 8H, $CH_{2/Bu}$), 0.74-0.57 (m, 20H, $CH_{2/Bu}$ + $CH_{3/Bu}$). $^{13}C\{^1H\}$ NMR (75 MHz, C_6D_6): δ = 151.4 & 151.2 (2×s, C_{Flu}), 144.9 (t, $^2J_{C,P}$ = 39 Hz, Fe*C*≡C), 141.7 & 141.3 (2×s, C_{Flu}), 139.7 & 137.8 (m, $C_{Ar/dppe}$), 134.4 (m, $CH_{Ar/dppe}$), 133.5, 132.0, 131.4, (3×s, CH_{Ar}/C_{Ar}), 129.5 & 129.2 (2×s, $CH_{Ar/dppe}$), 128.6-127.8 (m, CH_{Ar}/C_{Ar}/ $CH_{Ar/dppe}$), 126.5, 124.4, 123.2, 122.9, 120.5, 120.2 (6×s, CH_{Ar}/C_{Ar}), 119.6 (s, FeC≡*C*), 90.9 & 90.7 (2×s, C≡C), 88.1 (s, $C_5(CH_3)_5$), 55.4 (s, C_{Flu}), 40.6 (s, $CH_{2\text{-}Bu}$), 31.0 (m, $CH_{2/dppe}$), 26.4 (s, $CH_{2/Bu}$), 23.5 (s, $CH_{2/Bu}$), 14.0 (s, $CH_{3/Bu}$), 10.5 (s, $C_5(CH_3)_5$).

Synthesis of the Fe(III) Alkynyl Complexes

General Procedure. The Fe(II) alkynyl precursors (0.1 mmol) and 0.98 eq. [Fe(η^5-$C_5Me_5)_2$][PF_6] were dissolved in THF (20 mL). The dark orange reaction mixture was stirred for 90 min, becoming dark-green. Solvents and volatiles were removed in vacuo. The residue was taken up in CH_2Cl_2 (2 mL) and precipitated twice from *n*-pentane (15 mL), affording a green (**2a**[PF_6]) to dark green powder (**4a**[PF_6]/**5a**[PF_6]). This precipitate was subsequently washed with *n*-pentane (15 mL) and the supernatant was removed by decantation. After drying under high vacuum the cationic Fe(III) complex was obtained as a dark-green/brown powder.

[Fe(η^5-C_5Me_5)(κ^2-dppe){C≡C(1,4-C_6H_4)C≡C(2-$C_{13}H_7Bu_2$)}][PF_6] (2a[PF_6]). From 100 mg of **2a** and 33 mg of [Fe(η^5-$C_5Me_5)_2$][PF_6], 50 mg of green solid **2a**[PF_6] were isolated (44%).[24]

[Fe(η^5-C_5Me_5)(κ^2-dppe){C≡C(1,3-C_6H_4)C≡C(2-$C_{13}H_7Bu_2$)}][PF_6] (4a[PF_6]). From 100 mg of **4a** and 33 mg of [Fe(η^5-$C_5Me_5)_2$][PF_6], 75 mg of green solid **4a**[PF_6] were isolated (65%). IR (KBr, cm^{-1}): $\bar{\upsilon}$ = 2203 (w, C≡C); 2005 (s, FeC≡C), 1583 (m, C=C_{Ar}), 840 (vs, PF_6). $^{31}P\{^1H\}$ NMR (121 MHz, $CDCl_3$): δ = -144.4 (sept, $^1J_{P,F}$ = 706 Hz), P_{dppe} not observed. ^1H NMR (200 MHz, CD_2Cl_2): δ = 28.3 (s, 1H, CH_{Ph}), 8.3, 7.9 (s), 7.5 (s), 7.4 (m), 7.3 (s), 6.9 (s), 6.2 (s), 3.6 (s), 2.0-0.8 (m, $CH_{n/Bu}$ + $H_{Ph/dppe}$), -2.8 (s, 2H, $CH_{2/dppe}$), -10.5 (s, 15H,

$C_5(CH_3)_5$), -39.8 (broad s, 2H, CH_{Ph})), -40.9 (broad s, 1H, CH_{Ph}). ESR (THF, 80 K): g_1 = 2.441; g_2 = 2.034; g_3 = 1.976.

[Fe(η^5-C_5Me_5)(κ^2-dppe){C≡C(1,3,5-C_6H_3)[C≡C(2-$C_{13}H_7Bu_2$)]$_2$}][PF_6] (5a[PF_6]). From 150 mg of **5a** and 37 mg of [Fe(η^5-C_5Me_5)$_2$][PF_6], 100 mg of dark green solid **5a**[PF_6] were isolated (60%). IR (KBr, cm^{-1}): $\bar{\upsilon}$ = 2206 (w, C≡C); 2008 (s, FeC≡C), 1573 (m, C=C_{Ar}), 840 (vs, PF_6). $^{31}P\{^1H\}$ NMR (121 MHz, $CDCl_3$): δ = -144.4 (sept, $^1J_{P,F}$ = 710 Hz), P_{dppe} not observed. ^1H NMR (200 MHz, CD_2Cl_2): δ = 8.3, 7.9 (s), 7.5 (2 × s), 7.4 (m), 7.0 (s), 6.2 (s), 3.6 (s), 2.1-0.8 (m, $CH_{n/Bu}$ + $H_{Ph/dppe}$), -2.7 (s, 2H, $CH_{2/dppe}$), -10.4 (s, 15H, $C_5(CH_3)_5$), -37.1 (broad s, 1H, CH_{Ph}), -39.1 (s, 2H, CH_{Ph}). ESR (THF, 80 K): g_1 = 2.462; g_2 = 2.030; g_3 = 1.974.

Synthesis of the Ru(II) Mono-alkynyl Complexes

General Procedure. The organic alkyne (0.275 mmol) and the ruthenium precursor [Ru(κ^2-dppe)$_2$(Cl)][PF_6] (0.25 mmol) were dissolved in CH_2Cl_2 (10 mL) and stirred at 40 °C for 4 hours. The reaction mixture was then concentrated to ca. 5 mL under reduced pressure and the vinylidene salt was precipitated by addition of Et_2O. The precipitate was collected on a glass sintered funnel, washed with Et_2O (3 × 40 mL), *n*-hexane (3 × 40 mL) and dried in vacuo, providing the desired vinylidene complex as a gray powder (75-86% yield; see Supporting Information). This vinylidene complex (0.15 mmol) was then dissolved in CH_2Cl_2 (10 mL) and Et_3N (1.5mmol) was added. The resulting yellow reaction mixture was stirred for 15 min, filtered through a sintered glass funnel and the solid residue was further washed with CH_2Cl_2 (2 × 10 mL). The combined filtrates were concentrated under reduced pressure to ca. 5 mL and purified by column chromatography (basic alumina, 10 × 4 cm) eluting with CH_2Cl_2. The yellow band was collected and concentrated under reduced pressure to ca. 5 mL and CH_3OH was added to precipitate the desired complex. The precipitate was collected on a sintered glass funnel, washed with CH_3OH (3 × 40 mL), *n*-hexane (3 × 40 mL) and dried in vacuo, providing the corresponding alkynyl complex as a yellow-orange to orange powder.

***trans*-[Ru(κ^2-dppe)$_2$(Cl){C≡C(1,4-C_6H_4)C≡C(2-$C_{13}H_7Bu_2$)}] (2b).** From 227 mg of **2b-v**[PF_6] and 24 mL of NEt_3, 200 mg of **2b** were isolated (97%). X-ray quality crystals of this compound were grown from slow diffusion of n-hexane into a benzene solution. Anal. Calcd. for $C_{83}H_{77}ClP_4Ru$: C, 74.68%; H, 5.81%; found: C, 74.43%, H, 5.72%. HRMS (ESI): m/z calcd. for $C_{85}H_{80}NP_4Ru$ $[M–Cl+MeCN]^+$: 1340.4285; found: 1340.4281. IR (KBr, cm^{-1}): $\bar{\upsilon}$ = 2193 (w, C≡C); 2062 (s, Ru-C≡C). Raman (neat, cm^{-1}): $\bar{\upsilon}$ = 2192 (m, C≡C); 2062 (s, Ru-C≡C). $^{31}P\{^1H\}$ NMR (121 MHz, $CDCl_3$): δ = 49.1 (s, P_{dppe}). ^1H NMR (300 MHz, $CDCl_3$): δ = 7.84-7.62 (m, 3H, H_{Ar})), 7.58-7.42 (m, 12H, H_{Ar})), 7.39-7.29 (m, 12H, H_{Ar})), 7.24-7.14 (m, 7H, H_{Ar})), 7.10 – 6.89 (m, 15H, H_{Ar}), 6.57 (d, $^3J_{H,H}$ = 8.4 Hz, 2H, C_6H_4), 2.70 (m, 8H, $CH_{2/dppe}$), 1.99 (t, $^3J_{H,H}$ = 9.0 Hz, 4H, $CH_{2/Bu}$), 1.10 (m, 4H, $CH_{2/Bu}$), 0.71-0.56 (m, 10H, $CH_{2/Bu}$ + $CH_{3/Bu}$). $^{13}C\{^1H\}$ NMR (75 MHz, $CDCl_3$): δ = 150.9 & 150.6 (2×s, C_{Flu}), 140.9 & 140.5 (2×s, C_{Flu}), 136.2-134.1 (m, $C_{Ar/dppe}$), 145.2 (quint, $^2J_{C,P}$ = 16 Hz, Ru*C*≡C), 130.8, 130.4, 130.0, 128.9, 127.4, 127.2, 127.0, 126.9, 125.8, 122.9, 122.0, 119.9, 119.6 (m, C_{Ar}), 116.4 & 90.6 (2 × s, C≡C), 114.4 (broad s, RuC≡*C*), 55.0 (s, C_{Flu}), 40.2 (s, $CH_{2\text{-}Bu}$), 30.6 (m, $CH_{2/dppe}$), 25.9 & 24.1 (2 × s, $CH_{2/Bu}$), 13.8 (s, $CH_{3/Bu}$).

***trans*-[Ru(κ^2-dppe)$_2$(Cl){C≡C(1,3-C_6H_3)[C≡C(2-$C_{13}H_7Bu_2$)]$_2$}] (4b).** From 227 mg of **4b-v**[PF_6] and 24 mL of NEt_3, 180 mg of **4b** were isolated (90%). X-ray quality crystals of this compound were grown from

slow diffusion of *n*-hexane into a 1,2-$C_2H_2Cl_2$ solution. Anal. Calcd. for $C_{83}H_{77}ClP_4Ru \bullet ½C_2H_2Cl_2$: C, 72.93%; H, 5.68%; Found: C, 72.97%; H, 5.79%. HRMS (ESI): m/z calcd. for $C_{85}H_{80}NP_4Ru$ [M–Cl+MeCN]$^+$: 1340.4285; found: 1340.4288. IR (KBr, cm^{-1}): $\bar{\upsilon}$ = 2204 (w, C≡C); 2051 (s, Ru-C≡C). Raman (neat, cm^{-1}): $\bar{\upsilon}$ = 2207 (m, C≡C); 2046 (s, Ru-C≡C). $^{31}P\{^1H\}$ NMR (121 MHz, $CDCl_3$): δ = 49.3 (s, P_{dppe}). ^1H NMR (300 MHz, $CDCl_3$): δ = 7.77-7.68 (m, 3H, H_{Ar}), 7.59-7.44 (m, 11H, H_{Ar}), 7.42-7.32 (m, 11H, H_{Ar}), 7.24-7.13 (m, 8H, H_{Ar}), 7.13-6.93 (m, 16H, H_{Ar}), 6.66 (m, 2H, C_6H_4), 2.70 (m, 8H, $CH_{2/dppe}$), 2.01 (t, $^3J_{H,H}$ = 9.0 Hz, 4H, $CH_{2/Bu}$), 1.10 (m, 4H, $CH_{2/Bu}$), 0.71-0.57 (m, 10H, $CH_{2/Bu}$ + $CH_{3/Bu}$). $^{13}C\{^1H\}$ NMR (75 MHz, $CDCl_3$): δ = 151.0 & 150.8 (2 × s, C_{Flu}), 141.2 & 140.5 (2 × s, C_{Flu}), 136.5-135.9 (m, $C_{Ar/dppe}$), 134.5-134.3 (m, $C_{Ar/dppe}$), 130.5, 130.4, 129.8, 128.9, 127.6, 127.5, 127.3, 127.0, 125.9, 125.6, 123.0, 122.3, 122.0, 120.0, 119.7 (s & m, C_{Ar} & Ru*C*≡C), 112.8 (broad s, RuC≡*C*), 92.2 & 89.5 (2 × s, C≡C), 55.0 (s, C_{Flu}), 40.2 (s, $CH_{2\text{-}Bu}$), 30.6 (m, $CH_{2/dppe}$), 25.9 & 23.0 (2 × s, $CH_{2/Bu}$), 13.8 (s, $CH_{3/Bu}$).

***trans*-[Ru(κ^2-dppe)$_2$(Cl){C≡C(1,3,5-C_6H_4)C≡C(2-$C_{13}H_7Bu_2$)}] (5b).** From 267 mg of **5b-v**[PF_6] and 24 mL of NEt_3, 185 mg of **5b** were isolated (71%). X-ray quality crystals of this compound were grown from slow diffusion of *n*-hexane into a 1,2-dichloroethane solution. Anal. Calcd. for $C_{106}H_{101}ClP_4Ru$: C, 77.85%; H, 6.22%; found: C, 77.86%, H, 6.34%. HRMS (ESI): m/z calcd. for $C_{108}H_{104}NP_4Ru$ [M–Cl+MeCN]$^+$: 1640.6163; found: 1640.6163. IR (KBr, cm^{-1}): $\bar{\upsilon}$ = 2199 (w, C≡C); 2059 (s, Ru-C≡C). Raman (neat, cm^{-1}): $\bar{\upsilon}$ = 2207 (m, C≡C); 2059 (s, Ru-C≡C). $^{31}P\{^1H\}$ NMR (121 MHz, $CDCl_3$): δ = 49.0 (s, P_{dppe}). ^1H NMR (300 MHz, $CDCl_3$): δ = 7.81 – 7.69 (m, 4H, H_{Ar}), 7.63-7.55 (m, 4H, H_{Ar}), 7.50-7.34 (m, 23H, H_{Ar}), 7.29-7.18 (m, 7H, H_{Ar}), 7.12-6.97 (m, 17H, H_{Ar}), 6.68 (d, $^4J_{H,H}$ = 1.5 Hz, C_6H_4), 2.72 (m, 8H, $CH_{2/dppe}$), 2.01 (t, $^3J_{H,H}$ = 9.0 Hz, 8H, $CH_{2/Bu}$), 1.10 (m, 8H, $CH_{2/Bu}$), 0.72-0.57 (m, 20H, $CH_{2/Bu}$ + $CH_{3/Bu}$). $^{13}C\{^1H\}$ NMR (75 MHz, $CDCl_3$): □ = 151.0 & 150.8 (2 × s, C_{Flu}), 141.4 & 140.4 (2 × s, C_{Flu}), 136.4-134.1 (m, $C_{Ar/dppe}$), 130.0 (quint, $^2J_{C,P}$ = 15 Hz, Ru*C*≡C), 130.5, 129.2, 129.1, 128.5, 127.8, 127.6, 127.3, 127.2, 126.2, 123.2, 122.9, 122.0, 120.2, 119.8 (m, C_{Ar}), 112.0 (s, FeC≡*C*), 90.0 & 89.5 (2 × s, C≡C), 55.0 (s, C_{Flu}), 40.2 (s, $CH_{2\text{-}Bu}$), 30.6 (m, $CH_{2/dppe}$), 25.9 & 23.0 (2 × s, $CH_{2/Bu}$), 13.8 (s, $CH_{3/Bu}$).

Synthesis of the Ru(II) Bis-alkynyl Complexes

***trans*-[Ru(κ^2-dppe)$_2${C≡C(1,3,5-C_6H_4)C≡C(2-$C_{13}H_7Bu_2$)}$_2$] (6).** To a solution of the ruthenium precursor [Ru(κ^2-dppe)$_2$(Cl)][PF_6] (0.270 g, 0.25 mmol), the terminal alkyne **10** (0.369 g, 0.525 mmol) and $NaPF_6$ (0.126 mg, 0.75 mmol) in CH_2Cl_2 (25 mL), Et_3N (0.1 mL, 0.75 mmol) was added. After stirring at room temperature for 24 h, the reaction mixture was filtered through a sintered glass funnel and the residue was washed with CH_2Cl_2 (2 × 10 mL). The combined filtrates were concentrated under reduced pressure to ca. 5 mL and purified by column chromatography (basic alumina, 10 × 4 cm) eluting with CH_2Cl_2. The yellow band was collected and concentrated under reduced pressure to ca. 5 mL. CH_3OH was added to precipitate the bis-alkynyl complex and the precipitate was collected on a sintered glass funnel, washed with CH_3OH (3 × 40 mL) and *n*-hexane (3 × 40 mL), and dried in vacuo, providing the title complex as an yellow powder (0.52 g, 90%). Anal. Calcd. for $C_{160}H_{154}P_4Ru$: C, 83.48%; H, 6.74%; found: C, 83.09%, H, 6.91%. HRMS (ESI): m/z calcd. for $C_{160}H_{155}P_4Ru$ [M+H]$^+$: 2302.0123; found: 2302.0642. IR (KBr, cm^{-1}): $\bar{\upsilon}$ = 2206 (w, C≡C); 2050 (s, Ru-C≡C). Raman (neat, cm^{-1}): $\bar{\upsilon}$ = 2202 (m, C≡C); 2058 (s, Ru-C≡C). $^{31}P\{^1H\}$ NMR (121 MHz, $CDCl_3$): δ = 53.3 (s, P_{dppe}). ^1H NMR (300 MHz, $CDCl_3$): δ = 7.79-7.70 (m, 8H, H_{Ar}), 7.60-7.51 (m, 23H, H_{Ar}), 7.45-7.32 (m, 15H, H_{Ar}), 7.27 (s, 2H, H_{Ar}), 7.26-7.20 (m, 6H, H_{Ar}), 7.11-7.00 (m, 16H, H_{Ar}), 6.84 (s, $^4J_{H,H}$ = 1.4 Hz, 4H, C_6H_4), 2.69 (m, 8H, $CH_{2/dppe}$), 2.03 (t, $^3J_{H,H}$ = 9.0 Hz, 8H, $CH_{2/Bu}$), 1.11 (m, 16H, $CH_{2/Bu}$), 0.73-0.56 (m, 40H, $CH_{2/Bu}$ + $CH_{3/Bu}$).

$^{13}C\{^1H\}$ NMR (75 MHz, $CDCl_3$): δ = 151.0 & 150.8 (2 × s, C_{Flu}), 141.4 & 140.4 (2 × s, C_{Flu}), 136.9-133.2 (m, $C_{Ar/dppe}$), 136.1 (quint, $^2J_{C,P}$ = 15 Hz, Ru*C*≡C), 130.6, 128.9, 128.7, 127.6, 127.3, 127.0, 126.1, 123.0, 122.9, 121.8, 120.1, 119.7 (m, C_{Ar}), 115.7 (broad s, RuC≡*C*), 90.0 & 89.5 (2 × s, C≡C), 55.0 (s, C_{Flu}), 40.2 (s, *C*$H_{2\text{-}Bu}$), 31.4 (m, *C*$H_{2/dppe}$), 26.0 & 23.0 (2 × s, *C*$H_{2/Bu}$), 13.8 (s, *C*$H_{3/Bu}$).

***trans*-[Ru(κ^2-dppe)$_2$(C≡CFc){C≡C(1,3,5-C_6H_4)C≡C(2-$C_{13}H_7$-Bu_2)}] (7).** To a solution of **5b** (0.445 g, 0.25 mmol), ethynylferrocene (80 mg, 0.375 mmol) and $NaPF_6$ (0.170 g, 1.0 mmol) in CH_2Cl_2 (25 mL), Et_3N (0.11 mL, 1.0 mmol) was added. After stirring at room temperature for 24 h, the reaction mixture was filtered through a sintered glass funnel and the precipitate was washed with CH_2Cl_2 (2 × 10 mL). The combined filtrates were concentrated under reduced pressure to ca. 5 mL and purified by column chromatography (basic alumina, 10 × 4 cm), using CH_2Cl_2 as eluent. The orange band was collected and concentrated under reduced pressure to ca. 5 mL. CH_3OH was added to precipitate the bis-alkynyl complex. The precipitate was collected on a sintered glass funnel, washed with CH_3OH (3 × 40 mL), cold *n*-hexane (1 × 10 mL), and dried in vacuo, providing the title complex as an orange powder (0.377 g, 84%). Anal. Calcd. for $C_{118}H_{110}FeP_4Ru$: C, 78.35%; H, 6.13%; found: C, 78.00%, H, 6.51%. HRMS (ESI): m/z calcd. for $C_{118}H_{111}FeP_4Ru$ $[M+H]^+$: 1809.6029; found: 1809.6064. IR (KBr, cm^{-1}): $\bar{\upsilon}$ = 2204 (w, C≡C); 2056 (s, Ru-C≡C). Raman (neat, cm^{-1}): $\bar{\upsilon}$ = 2208 (m, C≡C); 2066 (s, Ru-C≡C). $^{31}P\{^1H\}$ NMR (121 MHz, C_6D_6): δ = 53.6 (s, P_{dppe}). ^1H NMR (300 MHz, C_6D_6): δ = 8.09 (s, 8H, H_{Ar}), 7.95 (s, 3H, H_{Ar}), 7.82 (m, 2H, H_{Ar}), 7.73-7.49 (m, 13H, H_{Ar}), 7.43-7.06 (m, 38H, H_{Ar}), 4.39, 4.29 & 4.22 (3 × s, 9H, HFc), 2.67 (m, 8H, C*H*$_{2/dppe}$), 2.07 (broad t, 8H, C*H*$_{2/Bu}$), 1.14 and 0.88 (m, 16H, C*H*$_{2/Bu}$), 0.71 (t, $^3J_{H,H}$ = 7.0 Hz, 12H, C*H*$_{3/Bu}$). $^{13}C\{^1H\}$ NMR (75 MHz, C_6D_6): δ = 151.4 & 151.3 (2 × s, C_{Flu}), 141.9 & 141.0 (2 × s, C_{Flu}), 139.0 (quint, $^2J_{C,P}$ = 15 Hz, Ru*C*≡C), 138.4-134.0 (m, $C_{Ar/dppe}$), 131.6, 131.3, 129.2, 129.0, 127.9, 127.6, 127.5, 126.5, 123.8, 123.2, 122.8 (m, C_{Ar}), 122.2 (quint, $^2J_{C,P}$ = 15 Hz, Ru*C*≡C), 120.5, 120.3 (m, C_{Ar}), 114.9 & 112.6 (2 × broad s, RuC≡*C*), 90.9 & 90.7 (2 × s, C≡C), 77.1-66.7 (4 × s, C_{Fc}), 53.4 (s, C_{Flu}), 40.6 (s, *C*$H_{2\text{-}Bu}$), 31.9 (m, *C*$H_{2/dppe}$), 26.4 & 23.5 (2 × s, *C*$H_{2/Bu}$), 14.0 (s, *C*$H_{3/Bu}$).

Luminescence Measurements. Luminescence measurements in solution were performed in dilute deoxygenated solutions (except in the case of ligands **9** and **10**) contained in air-tight quartz cells of 1 cm pathlength (*ca.* 10^{-6} M, optical density < 0.1) at room temperature (298 K), using an Edinburgh Instruments (FLS920) spectrometer equipped with a 450 W Xenon lamp and a Peltier-cooled Hamamatsu R928P photomultiplier tube in photon-counting mode. Fully corrected excitation and emission spectra were obtained with an optical density at $\lambda_{exc} \leq 0.1$ to minimize internal absorption. Luminescence quantum yields were measured according to literature procedures.[83] UV-vis absorption spectra used for the calculation of the luminescence quantum yields were recorded using a double beam Jasco V-570 spectrometer.

Spectroelectrochemistry. Solution UV/Vis/NIR spectra of the oxidized species were obtained at 243 K or 298 K by electrogeneration on a platinum mesh electrode in a 0.05 mm optically transparent thin-layer electrochemical (OTTLE) cell,[84] with a silver wire as pseudo-reference and a platinum wire as counter-electrode. Solutions were made up with [*n*-Bu_4N][PF_6] (0.20 M) in dry and deoxygenated CH_2Cl_2, and were kept under pure nitrogen.

DFT Calculations. Geometry optimizations were performed in vacuum with Orca 3.0[85] in the restricted (ground states) or unrestricted (triplet and quintet states) formalisms using the B3LYP* functional,[86] the def2-TZVP basis set,[87] and the empirical D3 dispersion correction.[88] Scalar relativistic effects were treated via the Zeroth-Order Regular Approximation (ZORA) method.[89] Minimum energy

crossing points[90] were optimized with Orca 3.0 at the same level of theory. Frequency calculations were performed to ascertain the nature of these points as minima. TD-DFT calculations (TDA) were performed at the same level of theory employing the ground state geometries and 40 roots were computed. Molecular orbitals were viewed and plotted with Gabedit.[91]

Z-scan Measurements. Third-order nonlinear optical properties were investigated as previously described,[92] but with some modifications. The laser system consisted of a Quantronix Integra-C3.5F pumping a Quantronix Palitra-FS optical parametric amplifier, tuned over a wavelength range from 500 nm to 800 nm. The output wavelength was confirmed by use of an Ocean Optics USB2000+ spectrometer. The system delivered 130 fs pulses with a 1 kHz repetition rate. Colored glass filters and a Thorlabs polarizing filter were used to remove unwanted wavelengths and the power adjusted by use of neutral density filters, attenuating it to the μJ/pulse range to obtain nonlinear phase shifts between 0.15 to 1.0 rad. The focal length of the lens used in the experiment was 75 mm, which gave 28-35 μm beam waists resulting in Rayleigh lengths sufficiently longer than that of the sample thickness that a "thin-sample" assumption was justified. Solutions of compounds in "as received" CH_2Cl_2 (see text), deoxygenated and distilled CH_2Cl_2, or deoxygenated and distilled THF, of 0.1 w/w% concentration in 1 mm glass cells were analyzed. Samples travelled down the Z-axis on a Thorlabs motorized stage between 5-45 mm. Data were collected by three Thorlabs photodiodes (500-900 nm with Si based detectors). Data from the detectors were fed into three channels of a Tektronix digital oscilloscope, collected with a custom LabVIEW program, and fitted with theoretical traces with a program that used equations derived by Sheik-Bahae et al.[93] A sample of the solvent was run at each wavelength to account for solvent and cell contribution to the Z-scan signals and the light intensity was determined from a Z-scan run on a 3 mm fused silica plate. A solution of each analyte was measured in deoxygenated and distilled CH_2Cl_2 of a concentration range of 0.2-0.5 wt% placed in a 1 mm glass cell; the real and imaginary components of the second hyperpolarizability (γ) of the materials were calculated assuming additivity of the nonlinear contributions of the solvent and the solute and the applicability of the Lorentz local field approximation. The values of the imaginary parts of γwere also converted into values of the two-photon absorption cross-sections σ_2.

Crystallography. Suitable crystals of **2b**•C_6H_6•C_6H_{14}, **4b**•1,2-$C_2H_2Cl_2$, **5b** and **III** (Supporting Information) were mounted on fine glass capillaries, and intensity data were collected on a Nonius KAPPA CCD diffractometer at 200 K using graphite-monochromated Mo-Kα radiation (λ = 0.71073 Å). N_t (total) reflections were measured by using psi and omega scans and were reduced to N_o unique reflections, with $F_o > 2\sigma(F_o)$ being considered to be observed. Semi-empirical absorption corrections based on symmetry-equivalent and repeat reflections were applied.[94] The structures were solved using direct methods and observed reflections were used in least-squares refinement on F^2, with anisotropic thermal parameters refined for non-hydrogen atoms. Hydrogen atoms were constrained in calculated positions and refined with a riding model. Structure solutions and refinements were performed by using the programs SHELXS-97[95] and SHELXL-2014[96] through the graphical interface Olex2.[97] Atomic scattering factors were taken from the literature.[98] Views of **2b**, **4b** and **5b** were generated with ORTEP.[99]

Variata. In **2b**; anisotropic displacement parameter constraints were applied to one lattice benzene molecule (atoms C84 – C89), and the geometry was constrained to fit a regular hexagon. In **5b**;

anisotropic displacement parameter constraints were applied to several n-butyl groups (C76 – C83 and C99 – C106). Bond distance restraints were also applied to a n-butly group (C76 – C83). Disordered lattice solvent could not be successfully modelled, and was therefore removed from the refinement using the smtbx_masks function of Olex2.[97]

Supporting Information. Synthesis and characterization of **8**, **9** and **10**. Crystallographic, spectroscopic, voltammetric, computational and Z-scan data on selected complexes. ^{1}H NMR and ESR spectra of **4b**$[PF_6]_2$ and **5b**$[PF_6]$. CIF files for **2b**, **4b**, **5b** and **III** have been deposited at the Cambridge Crystallographic Data Center and were allocated the deposition numbers CCDC 1839400-1839403, respectively. Ordering information is given on any current masthead page.

Acknowledgements. The CNRS (PICS program N° 7106 and LIA N° 1194) is acknowledged for financial support. A.T. and G.G. thank the Region Bretagne for a Ph.D. grant. FP thanks Bertrand Lefeuvre (ISCR) for experimental help in recording the Raman spectra M.G.H. thanks the Australian Research Council (ARC) for financial support and M.P.C. thanks the ARC for an Australian Research Fellowship. We also acknowledge the HPC resources from CALMIP (Toulouse).

REFERENCES

(1) Balzani, V.; de Silva, A. P. Electron Transfer in Chemistry; Wiley-VCH, 2000; Vol. 5.

(2) Marques-Gonzalez, S.; Parthey, M.; Yufit, D. S.; Howard, J. A. K.; Kaupp, M.; Low, P. J. Combined Spectroscopic and Quantum Chemical Study of [trans-$Ru(CCC_6H_4R_{14})_2(dppe)_2]^{n+}$ and [trans-$Ru(CCC_6H_4R_{14})(CCC_6H_4R_{24})(dppe)2]^{n+}$ (n = 0, 1) Complexes: Interpretations beyond the Lowest Energy Conformer Paradigm, *Organometallics* **2014**, *33*, 4947-4963.

(3) (a) Vacher, A.; Barrière, F.; Lorcy, D. Ferrocene and Tetrathiafulvalene Redox Interplay across a Bisacetylide-Ruthenium Bridge, *Organometallics* **2013**, 6130-6135; (b) Akita, M.; Koike, T. Chemistry of polycarbon species: from clusters to molecular devices, *J. Chem. Soc., Dalton Trans.* **2008**, 3523-3530; (c) Rigaut, S.; Touchard, D.; Dixneuf, P. H. Redox active architectures and carbon-rich ruthenium complexes a models for molecular wires In *Redox Systems Under Nano-space Control*; Hirao, T., Ed.; Springer Verlag: Heidelberg, 2006; (d) Ren, T. Diruthenium sigma-alkynyl compounds: a new class of conjugated organometallics, *Organometallics* **2005**, *24*, 4854-4870; (e) Low, P. J. Metal complexes in molecular electronics: progress and possibilities, *J. Chem. Soc., Dalton Trans.* **2005**, 2821-2824.

(4) Paul, F.; Lapinte, C. Organometallic molecular wires and other nanoscale-sized devices. An approach using the organoiron (dppe)Cp*Fe building block, *Coord. Chem. Rev.* **1998**, *178/180*, 431-509.

(5) (a) Lyu, S.; Farré, Y.; Ducasse, L.; Pellegrin, Y.; Toupance, T.; Olivier, C.; Odobel, F. Push–pull ruthenium diacetylide complexes: new dyes for p-type dye-sensitized solar cells, *RSC Adv.* **2016**, *6*, 19928-19936; (b) De Sousa, S.; Lyu, S.; Ducasse, L.; Toupance, T.; Olivier, C. Tuning visible-light

absorption properties of Ru–diacetylide complexes: simple access to colorful efficient dyes for DSSCs, *J. Mater. Chem. A* **2015**, *3*, 18256-18264.

(6) De Sousa, S.; Ducasse, L.; Kauffmann, B.; Toupance, T.; Olivier, C. Functionalization of a Ruthenium–Diacetylide Organometallic Complex as a Next-Generation Push–Pull Chromophore, *Chem. Eur. J.* **2014**, *20*, 7017-7024.

(7) (a) Merhi, A.; Zhang, X.; Yao, D.; Drouet, S.; Mongin, O.; Paul, F.; Williams, J. A. G.; Fox, M. A.; Paul-Roth, C. O. New Donor-Acceptor Conjugates based on a Trifluorenylporphyrin linked to a Redox–Switchable Ruthenium Unit, *Dalton Trans.* **2015**, *44*, 9470-9485; (b) Di Piazza, E.; Norel, L.; Costuas, K.; Bourdolle, A.; Maury, O.; Rigaut, S. d-f Heterobimetallic Association between Ytterbium and Ruthenium Carbon-Rich Complexes: Redox Commutation of NIR Luminescence. , *J. Am. Chem. Soc.* **2011**, *133* 6174-6775.

(8) Norel, L.; Di Piazza, E.; Feng, M.; Vacher, A.; He, X.; Roisnel, T.; Maury, O.; Rigaut, S. Lanthanide Sensitization with Ruthenium Carbon-Rich Complexes and Redox Commutation of Near-IR Luminescence, *Organometallics* **2014**, *33* 4824-4835.

(9) Murai, M.; Sugimoto, M.; Akita, M. Dalton Trans. 2013, 42, 1610 Murai, M.; Sugimoto, M.; Akita, M. Zinc-porphyrins functionalized with redox-active metal peripherals: enhancement of $d\pi$-$p\pi$ interaction leading to unique assembly and redox-triggered remote switching of fluorescence, *Dalton Trans.* **2013**, *42*, 161088-16120.

(10) de Montigny, F.; Argouarch, G.; Roisnel, T.; Toupet, L.; Lapinte, C.; Lam, S. C.-F.; Tao, C.-H.; Yam, V. W.-W. Syntheses, structures, and properties of some piano-stool iron acetylides bearing a functional anthracenyl group, *Organometallics* **2008**, *27*, 1912-1923.

(11) Wong, K. M.-C.; Lam, S. C.-F.; Ko, C.-C.; Zhu, N.; Yam, V. W.-W.; Roué, S.; Lapinte, C.; Fathallah, S.; Costuas, K.; Kahlal, S.; Halet, J.-F. Electroswitchable photoluminescence activity: Synthesis, spectroscopy, electrochemistry, photophysics, and X-ray crystal and electronic structure of $[Re(bpy)(CO)_3(CC\text{-}C_6H_4\text{-}CC)Fe(C_5Me_5)\text{-}(dppe)][PF_6]_n$ (n = 0,1), *Inorg. Chem.* **2003**, *42*, 7086-7097.

(12) Grelaud, G.; Cifuentes, M. P.; Paul, F.; Humphrey, M. G. Group 8 Metal Alkynyl Complexes for Nonlinear Optics, *J. Organomet. Chem.* **2014**, *751*, 181-200 and refs therein.

(13) (a) Bellier, Q.; Makarov, N. S.; Bouit, P.-A.; Rigaut, S.; Kamada, K.; Feneyrou, P.; Berginc, G.; Maury, O.; Perry, J. W.; Andraud, C. Excited state absorption: a key phenomenon for the improvement of biphotonic based optical limiting at telecommunication wavelengths, *Phys. Chem. Chem. Phys.* **2012**, *14*, 15299-15307; (b) Samoc, M.; Morrall, J.-P.; Dalton, G. T.; Cifuentes, M. P.; Humphrey, M. G. Two-photon and three-photon absorption in an organometallic dendrimer, *Angew. Chem., Int. Ed. Engl.* **2007**, *46*, 731-733; (c) Long, N. J.; Williams, C. K. Metal alkynyl sigma complexes: synthesis and materials, *Angew. Chem., Int. Ed. Engl.* **2003**, *42*, 2586-2617.

(14) Roberts, R. L.; Schwich, T.; Corkery, T. C.; Cifuentes, M. P.; Green, K. A.; Farmer, J. D.; Low, P. J.; Marder, T. B.; Samoc, M.; Humphrey, M. G. Organometallic Complexes for Nonlinear Optics. 45. Dispersion of the Third-Order Nonlinear Optical Properties of Triphenylamine-Cored Alkynylruthenium Dendrimers, *Adv. Mat.* **2009**, *21*, 2318-2322.

(15) Cifuentes, M. P.; Humphrey, M. G.; Morrall, J. P.; Samoc, M.; Paul, F.; Roisnel, T.; Lapinte, C. Third-order nonlinear optical properties of some electron-rich iron mono- and trinuclear alkynyl complexes, *Organometallics* **2005**, *24*, 4280-4288.

(16) Morrall, J. P.; Dalton, G. T.; Humphrey, M. G.; Samoc, M. Organotransition metal complexes for nonlinear optics, *Adv. Organomet. Chem.* **2008**, *55*, 61-136.

(17) Powell, C. E.; Humphrey, M. G. Nonlinear optical properties of transition metal acetylides and their derivatives, *Coord. Chem. Rev.* **2004**, *248*, 725-756.

(18) (a) Shen, C.; He, X.; Toupet, L.; Norel, L.; Rigaut, S.; Crassous, J. Dual Redox and Optical Control of Chiroptical Activity in Photochromic Dithienylethenes Decorated with Hexahelicene and Bis-Ethynyl-Ruthenium Units, *Organometallics* **2018**, *37*, 697-705; (b) Srebro, M.; Anger, E.; B. Moore, I.; Vanthuyne, N.; Roussel, C.; Réau, R.; Autschbach, J.; J. Crassous Ruthenium-Grafted Vinylhelicenes: Chiroptical Properties and Redox Switching, *Chem. Eur. J.* **2015**, *21*, 17100-17115; (c) Anger, E.; Srebro, M.; Vanthuyne, N.; Toupet, L.; Rigaut, S.; Roussel, C.; Autschbach, J.; Crassous, J.; Réau, R. *J. Am. Chem. Soc.* **2012**, *134*, 15628-15630.

(19) Shen, C.; Loas, G.; Srebro-Hooper, M.; Vanthuyne, N.; Toupet, L.; Cador, O.; Paul, F.; Navarrete, J. T. L.; Ramírez, F. J.; Nieto-Ortega, B.; Casado, J.; Autschbach, J.; Vallet, M.; Crassous, J. Iron-alkynyl-helicenes: redox-triggered chiroptical tuning in the vibrational and telecommunication domain, *Angew. Chem. Int. Ed.* **2016**, *55*, 8062-8066.

(20) Nijegorodov, N. I.; Downey, W. S. The influence of planarity and rigidity on the absorption and fluorescence parameters and intersystem crossing rate constant in aromatic molecules, *J. Phys. Chem.* **1994**, *98*, 5639-5643.

(21) Belfield, K. D.; Bondar, M. V.; Hernandez, F. E.; Przhonska, O. V.; Yao, S. Two-Photon Absorption Cross Section Determination for Fluorene Derivatives: Analysis of the Methodology and Elucidation of the Origin of the Absorption Processes, *J. Phys. Chem. B* **2007**, *111*, 12723-12729.

(22) (a) Matsusaka, Y.; Shitaya, S.; Nomura, K.; Inagaki, A. Synthesis of Mono-, Di-, and Trinuclear Rhodium Diphosphine Complexes Containing Light-Harvesting Fluorene Backbones, *Inorg. Chem.* **2017**, *56*, 1027-1030; (b) Chinelatto, L. S., Jr; del Barrioa, J.; Pinol, M.; Oriol, L.; M.A. Matranga; Santo, M. P. D.; Barberi, R. Oligofluorene blue emitters for cholesteric liquid crystal lasers, *J. Photochem. Photobiol. A: Chemistry* **2010**, *210*, 130-139; (c) Feng, X. J.; Wu, P. L.; Tam, H. L.; Li, K. F.; Wong, M. S.; Cheah, K. W. Fluorene-based pi-conjugated oligomers for efficient three-photon excited photoluminescence and lasing, *Chem. Eur. J.* **2009**, *15*, 11681-11691; (d) Ren, S.; Cheng, J.; Zeng, D.; Zhu, W.; Sun, J.; Du, J.; Xu, E.; Zhong, H.; Liu, Y.; Fang, Q. A new pi-conjugated star-shaped polymer comprising of full fluorene units: an efficent blue emitter without reduction of color purity undergoing an annealing, *Synth. Metals* **2009**, *159*, 29-35; (e) Mongin, O.; Krishna, T. R.; Werts, M. H. V.; Caminade, A.-M.; Majoral, J.-P.; Blanchard-Desce, M. A modular approach to two-photon absorbing organic nanodots: brilliant dendrimers as an alternative to semiconductor quantum dots, *Chem. Commun.* **2006**, 915-917; (f) Terenziani, F.; Katan, C.; Badaeva, E.; Tretiak, S.; Blanchard-Desce, M. Enhanced Two-Photon Absorption of Organic Chromophores: Theoretical and Experimental Assessments (p NA), *Adv. Mater.* **2008**, *20*, 4541-4678; (g) Rouxel, C.; Charlot, M.; Mongin, O.; Krishna, T. R.; Caminade, A.-M.; Majoral, J.-P.; Blanchard-Desce, M. From Graftable Biphotonic

Chromophores to Water-Soluble Organic Nanodots for Biophotonics: The Importance of Environmental Effects, *Chem. Eur. J.* **2012**, *18*, 16450-16462; (h) Silly, M. G.; Porres, L.; Mongin, O.; Chollet, P. A.; Blanchard-Desce, M. Optical limiting in the red–NIR range with soluble two-photon absorbing molecules, *Chem. Phys. Lett.* **2003**, *379*, 74-80; (i) Liu, R.; Azenkeng, A.; Li, Y.; Sun, W. Long-lived platinum(II) diimine complexes with broadband excited-state absorption: efficient nonlinear absorbing materials, *Dalton Trans.* **2012**, *41*, 12353-12357; (j) Hong, J. M.; Cho, H. N.; Kim, D. Y.; Kim, C. Y. Synthesis and Luminescence Studies of Poly(fluorenylene ethynylen)s, *Synth. Met.* **1999**, *102*, 933-934.

(23) Lewis, J.; Raithby, P. R.; Wong, W.-Y. Synthesis of new bis(acetylide)-substituted fluorene derivatives and the bimetallic and polymeric complexes, *J. Organomet. Chem.* **1998**, *556*, 219-228.

(24) Malvolti, F.; Rouxel, C.; Triadon, A.; Grelaud, G.; Richy, N.; Mongin, O.; Blanchard-Desce, M.; Toupet, L.; Abdul Razak, F. I.; Stranger, R.; M. Samoc; Yang, X.; Wang, G.; Barlow, A.; Cifuentes, M. P.; Humphrey, M. G.; Paul, F. 2,7-Fluorenediyl-bridged Complexes Containing Electroactive "Fe(η^5-C_5Me_5)(κ^2-dppe)C≡C-" Endgroups: Molecular Wires and Remarkable Nonlinear Electrochromes, *Organometallics* **2015**, *34*, 5418-5437.

(25) Malvolti, F.; Rouxel, C.; Grelaud, G.; Toupet, L.; Roisnel, T.; Yang, X.; Wang, G.; Barlow, A.; Abdul Razak, F. I.; Stranger, R.; Cifuentes, M. P.; Humphrey, M. G.; Mongin, O.; Blanchard-Desce, M.; Paul-Roth, C. O.; Paul, F. Iron and Ruthenium Alkynyl Complexes with 2-Fluorenyl Groups: Some Linear and Nonlinear Optical Absorption Properties, *Eur. J. Inorg. Chem.* **2016**, 3868-3882.

(26) For ferrocene-containing analogues, see: (a) Wong, W.-Y.; Lu, G.-L.; Choi, K.-H.; Guo, Y.-H. Carbon-rich organometallics: synthesis and characterization of new ferrocenyl end-capped bis(butadiynyl) fluorene derivatives, *J. Organomet. Chem.* **2005**, *690*, 177-186; (b) Wong, W.-Y.; Lu, G.-L.; Ng, K.-F.; Wong, C.-K.; Choi, K.-H. Synthesis, structures and electrochemistry of bis(alkynylferrocene) complexes with fluorene spacers, *J. Organomet. Chem.* **2001**, *637-639*, 159-166.

(27(a) Drouet, S.; Merhi, A.; Grelaud, G.; Cifuentes, M. P.; Humphrey, M. G.; Matczyszyn, K.; Samoc, M.; Toupet, L.; Paul-Roth, C. O.; Paul, F. Enhanced two-photon absorption cross-sections of zinc(II) tetraphenylporphyrins peripherally substituted with d6-metal alkynyl complexes, *New J. Chem.* **2012**, *36*, 2192-2195; (b) Drouet, S.; Merhi, A.; Yao, D.; Cifuentes, M. P.; Humphrey, M. G.; Wielgus, M.; Olesiak-Banska, J.; Matczyszyn, K.; Samoc, M.; Paul, F.; Paul-Roth, C. O. Cubic Nonlinear Optical Properties of New Zinc Tetraphenyl Porphyrins Peripherally Functionalized with Electron-rich Ru(II) Alkynyl Substituents, *Tetrahedron* **2012**, *68*, 10351-10359; (c) Green, K. A.; Simpson, P. V.; Corkery, T. C.; M. P. Cifuentes; Samoc, M.; Humphrey, M. G. Divergent Synthesis of Ruthenium Alkynyl Dendrimers and a Two-Photon Absorption Cross-Section Dendritic Effect, *Macromol. Rapid Commun.* **2012**, *33*, 573-578; (d) Samoc, M.; Corkery, T. C.; McDonagh, A. M.; Cifuentes, M. P.; Humphrey, M. G. "Ref MGH", *Aust. J. Chem.* **2011**, *64*, 1269-1273; (e) Jeffery, C. J.; Cifuentes, M. P.; Willis, A. C.; Samoc, M.; Humphrey, M. G. "Ref MGH", *Macromol. Rapid Commun.* **2010**, *31*, 846-849; (f) Green, K. A.; Cifuentes, M. P.; Corkery, T. C.; Samoc, M.; Humphrey, M. G. Switching the Cubic Nonlinear Optical Properties of an Electro-, Halo-, and Photochromic Ruthenium Alkynyl Complex Across Six States, *Angew. Chem., Int. Ed. Engl.* **2009**, *48*, 7867-7870; (g) Dalton, G. T.; Cifuentes, M. P.; Watson, L. A.; Petrie, S.; Stranger, R.; Samoc, M.; Humphrey, M. G. Organometallic Complexes for Nonlinear Optics. 42.1 Syntheses, Linear, and Nonlinear Optical Properties of Ligated Metal-Functionalized

Oligo(p-phenyleneethynylene)s, *Inorg. Chem.* **2009**, *48*, 6534-6547; (h) Babgi, B.; Rigamonti, L.; Cifuentes, M. P.; Corkery, T. C.; Randles, M. D.; Schwich, T.; Petrie, S.; Stranger, R.; Teshome, A.; Asselberghs, I.; Clays, K.; Samoc, M.; Humphrey, M. G. Length-Dependent Convergence and Saturation Behavior of Electrochemical, Linear Optical, Quadratic Nonlinear Optical, and Cubic Nonlinear Optical Properties of Dipolar Alkynylruthenium Complexes with Oligo(phenylene-ethynylene) Bridges, *J. Am. Chem. Soc.* **2009**, *131*, 10293-10307; (i) Dalton, G. T.; Cifuentes, M. P.; Petrie, S.; Stranger, R.; Humphrey, M. G.; Samoc, M. Independent switching of cubic nonlinear optical properties in a ruthenium alkynyl cruciform complex by employing protic and electrochemical stimuli, *J. Am. Chem. Soc.* **2007**, *129*, 11882-11883; (j) Powell, C. E.; Morrall, J. P.; Ward, S. A.; Cifuentes, M. P.; Notaras, E. G. A.; Samoc, M.; Humphrey, M. G. Dispersion of the third-order nonlinear optical properties of an organometallic dendrimer, *J. Am. Chem. Soc.* **2004**, *126*, 12234-12235.

(28) He, G. S.; Tan, L.-S.; Zheng, Q.; Prasad, P. N. Multiphoton Absorbing Materials: Molecular Designs, Characterizations, and Applications, *Chem. Rev.* **2008**, *108*, 1245-1330.

(29) Schäfer, J.; Holzapfel, M.; Mladenova, B.; Kattnig, D.; Krummenacher, I.; Braunschweig, H.; Grampp, G.; Lambert, C. Hole Transfer Processes in meta- and para-Conjugated Mixed Valence Compounds: Unforeseen Effects of Bridge Substituents and Solvent Dynamics, *J. Am. Chem. Soc.* **2017**, *139*, 6200-6209.

(30) Weyland, T.; Costuas, K.; Toupet, L.; Halet, J.-F.; Lapinte, C. Organometallic mixed-valence systems. Two-center and three-center compounds with meta connections around a central phenylene ring, *Organometallics* **2000**, *19*, 4228-4239.

(31) Ibn Ghazala, S.; Paul, F.; Toupet, L.; Roisnel, T.; Hapiot, P.; Lapinte, C. Di-organoiron Mixed Valent Complexes featuring "(η^2-dppe)(κ^5-C_5Me_5)Fe" Endgroups: Smooth Class-III to Class-II Transition induced by Successive Insertion of 1,4-Phenylene units in a Butadiyne-Diyl Bridge, *J. Am. Chem. Soc.* **2006**, *128*, 2463-2476.

(32) In these equations k_{lum} is the luminescence decay rate, k_{eT} is the electron quenching rate, while k_{NR} corresponds to the decay rate of the other non-radiative processes. $\Delta G^{\neq}$ is the activation energy for the redox quenching reaction, which depends on the reorganization energy (λ) and the driving force of the electron transfer process (ΔG_{eT}), while H_{ab} is the electronic coupling between the redox sites, T is the temperature, and k_B is the Boltzmann constant.[33]

(33) Astruc, D. Electron Transfer and Radical Processes in Transition-Metal Chemistry; VCH Publishers, Inc.: New York, 1995.

(34) Bazourkas, M.; Blanchard-desce, M. Molecular engineeing of push-pull dipolar and quadrupolar molecules for two-photon absorption: a multi valence-bond states approach, *J. Chem. Phys.* **2000**, *113*, 3951-3959.

(35) The starting alkyne (9,9-dibutyl-2-Flu)C≡CH was also structurally characterized. It crystallizes in the triclinic system: space group, P-1; a, 12.084(2) Å; b, 13.285(3) Å; c, 13.351(3) Å; α, 74.96(3)°; β, 64.76(3)°; γ, 81.34(3)°; V = 1870.4(8) Å^3; Z = 4; R = 0.0498 (see Supporting Information).

(36) Denis, R.; Toupet, L.; Paul, F.; Lapinte, C. Electron-Rich Piano-stool Iron sigma-Acetylides bearing a Functional Aryl Group. Synthesis and Characterization of Fe(II) and Fe(III) Complexes, *Organometallics* **2000**, *19*, 4240-4251.

(37) Gauthier, N.; Tchouar, N.; Justaud, F.; Argouarch, G.; Cifuentes, M. P.; Toupet, L.; Touchard, D.; Halet, J.-F.; Rigaut, S.; Humphrey, M. G.; Costuas, K.; Paul, F. Bonding and electron delocalization in Ru(III) arylacetylide radicals [*trans*-Cl(κ^2-dppe)$_2$RuCC(4-C_6H_4X)]$^+$ (X = NO_2, C(O)H, C(O)-Me, F, H, OMe, NMe_2): misleading aspects of the ESR anisotropy, *Organometallics* **2009**, *28*, 2253-2266.

(38) Bruce, M. I. Transition metal complexes containing allenylidene, cumulenylidene, and related ligands, *Chem. Rev.* **1998**, *98*, 2797-2858.

(39) Touchard, D.; Haquette, P.; Guesmi, S.; Le Pichon, L.; Daridor, A.; Toupet, L.; Dixneuf, P. H. Vinylidene-, Alkynyl-, and trans-Bis(alkynyl)ruthenium Complexes. Crystal Structure of trans-[Ru(NH_3)(CC-Ph)($Ph_2PCH_2CH_2PPh_2$)$_2$]PF_6, *Organometallics* **1997**, *16*, 3640-3648.

(40) McDonagh, A. R.; Cifuentes, M. P.; Whittall, I. R.; Humphrey, M. G.; Samoc, M.; Luther-Davies, B.; Hockless, D. C. R. Organometallic complexes for nonlinear optics. VII. Cubic optical nonlinearities of octahedral trans-bis{bis(diphenylphosphino)methane}ruthenium acetylide complexes; x-ray crystal structure of trans-[Ru(C≡CPh)(4-C≡C$C_6H_4NO_2$)(dppm)$_2$], *J. Organomet. Chem.* **1996**, *526*, 99-103.

(41) Paul, F.; Ellis, B. J.; Bruce, M. I.; Toupet, L.; Roisnel, T.; Costuas, K.; Halet, J.-F.; Lapinte, C. Bonding and substituent effects in electron-rich mononuclear ruthenium sigma-arylacetylides of formula [(eta^2-dppe) (eta^5-C_5Me_5)Ru(CC)-1,4-(C_6H_4)X][PF_6]$_n$ (n = 0,1; X = NO_2, CN, F, H, OMe, NH_2), *Organometallics* **2006**, *25*, 649-665.

(42) (a) Hurst, S. K.; Cifuentes, M. P.; Morrall, J. P. L.; Lucas, N. T.; Whittall, I. R.; Humphrey, M. G.; Asselberghs, I.; Persoons, A.; Samoc, M.; Luther-Davies, B.; Willis, A. C. Organometallic complexes for nonlinear optics. 22. Quadratic and cubic hyperpolarizabilities of trans-bis(bidentate phosphine)ruthenium sigma-arylvinylidene and sigma-arylalkynyl complexes, *Organometallics* **2001**, *20*, 4664-4675; (b) Morrall, J. P.; Cifuentes, M. P.; Humphrey, M. G.; Kellens, R.; Robijns, E.; Asselberghs, I.; Clays, K.; Persoons, A.; Samoc, M.; Willis, A. C. Organometallic complexes for nonlinear optics. Part 36. Quadratic and cubic optical nonlinearities for 4-fluorophenylethynyl- and 4-nitro-(E)-stilbenylethynylruthenium complexes, *Inorg. Chim. Acta* **2006**, *359*, 998-1005 and refs therein.

(43) Paul, F.; Toupet, L.; Thépot, J.-Y.; Costuas, K.; Halet, J.-F.; Lapinte, C. Electron-Rich Piano-stool Iron sigma-Acetylides. Electronic Structure of Arylalkynyl Fe(III) Radical Cations, *Organometallics* **2005**, *24*, 5464-5478.

(44) Paul, F.; da Costa, G.; Bondon, A.; Gauthier, N.; Sinbandhit, S.; Toupet, L.; Costuas, K.; Halet, J.-F.; Lapinte, C. Spin delocalization in Electron-Rich Iron(III) Piano-stool Acetylides. An Experimental (NMR) and Theoretical (DFT) Investigation, *Organometallics* **2007**, *26*, 874-896.

(45) Grelaud, G.; Cifuentes, M. P.; Schwich, T.; Argouarch, G.; Petrie, S.; Stranger, R.; Paul, F.; Humphrey, M. G. Multi-State Redox-Active Metallated-Triarylamines, *Eur. J. Inorg. Chem.* **2012**, 65-75.

(46) (a) Grelaud, G.; Gauthier, N.; Luo, Y.; Paul, F.; Fabre, B.; Barrière, F.; Ababou-Girard, S.; Roisnel, T.; Humphrey, M. G. Redox-active Molecular Wires Derived From Dinuclear Ferrocenyl/Ruthenium(II) Alkynyl Complexes: Covalent Attachment to Hydrogen-Terminated Silicon Surfaces, *J. Phys. Chem. C* **2014**, *118*, 3680-3695; (b) Colbert, M. C.; Lewis, J.; Long, N. J.; Raithby, P. R.; White, A. J. P.; Williams, D. J. Synthetic, structural, electrochemical and electronic characterization of heterobimetallic bis(acetylide) ferrocene complexes, *J. Chem. Soc., Dalton. Trans.* **1997**, 99-104; (c) Lebreton, C.; Touchard, D.; Le Pichon, L.; Daridor, A.; Toupet, L.; Dixneuf, P. H. Mono- and bis-alkynyl ruthenium(II) complexes containing the ferrocenyl moiety; crystal structure of trans-$[Ru(CCC_5H_5FeC_5H_5)_2(Ph_2PCH_2CH_2PPh_2)_2]$ and electrochemical studies, *Inorg. Chim. Acta* **1998**, *272*, 188-196.

(47) Poriel, C.; Liang, J.-J.; Rault-Berthelot, J.; Barrière, F.; Cocherel, N.; Slawin, A. M. Z.; Horhant, D.; Virboul, M.; Alcaraz, G.; Audebrand, N.; Vignau, L.; Huby, N.; Wantz, G.; Hirsch, L. Dispirofluorene–Indenofluorene Derivatives as New Building Blocks for Blue Organic Electroluminescent Devices and Electroactive Polymers, *Chem. Eur. J.* **2007**, *13*, 10055-10069.

(48) Courmarcel, J.; Le Gland, G.; Toupet, L.; Paul, F.; Lapinte, C. Versatile Reactions of a *para*-Bromophenylacetylide Iron(II) derivative and X-ray Structure of the Fluoro Analogue. Synthesis of New Redox-active Organoiron(II) Synthons, *J. Organomet. Chem.* **2003**, *670*, 108-122.

(49) Weller, A. Photoinduced Electron Transfer in Solution:Exciplex and Radical Ion Pair Formation Free Enthalpies and their Solvent Dependence, *Z.. Phys. Chem. N. F.* **1982**, *133*, 93-98.

(50) In this equation, the electron donor (D) is the Fe(II) center and the acceptor (A) the fluorene group, e is the electron charge, ε_0 is the dielectric constant in vacuum, ε is the relative dielectric constant and d is the distance between the positive and negative charges in the CT state. The latter was obtained from the distance between the metal center and the midpoint of the fluorene unit for **2a-b** and **4a-b**. For **5a-b**, **6** and **7**, where several fluorenyl units are present, the mean distance was employed. Estimates of these distances were obtained from the available X-ray data for **1a**,[24] **2b**, **4b** and **5b**.

(51) In this equation the electron donor (D) is now the fluorene group and the acceptor (A) the Fe(III) center.

(52) Albright, T. A.; Burdett, J. K.; Wangbo, J.-H. *Orbital Interaction in Chemistry*; Wiley-Interscience: New-York, 1985.

(53) Gauthier, N.; Olivier, C.; Rigaut, S.; Touchard, D.; Roisnel, T.; Humphrey, M. G.; Paul, F. Intramolecular Optical Electron-transfer in Mixed-Valent Dinuclear Iron-Ruthenium Complexes Featuring a 1,4-Diethynylaryl Spacer, *Organometallics* **2008**, *27*, 1063-1072.

(54) (a) Cuffe, L.; Hudson, R. D. A.; Gallagher, J. F.; Jennings, S.; McAdam, C. J.; Connelly, R. B. T.; Manning, A. R.; Robinson, B. H.; Simpson, J. Synthesis, structures and redox chemistry of ethenyl and ethynyl ferrocene polyaromatic dyads, *Organometallics* **2005**, *24*, 2051-1562; (b) Barlow, S.; Marder, S. R. Electronic and optical properties of conjugated group 8 metallocene derivatives, *Chem. Commun.* **2000**, 1555-1562.

(55) Powell, C. E.; Cifuentes, M. P.; Morrall, J. P.; Stranger, R.; Humphrey, M. G.; Samoc, M.; Luther-Davies, B.; Heath, G. A. Organometallic complexes for nonlinear optics. 30. Electrochromic linear and nonlinear optical properties of alkynylbis(diphosphine)-ruthenium complexes, *J. Am. Chem. Soc.* **2003**, *125*, 602-610.

(56) (a) Li, Z.; Beatty, A. M.; Sharma, S.; Fehlner, T. P. Molecular QCA cells. 1. Structure and functionalization of an unsymmetrical dinuclear mixed-valence complex for surface binding, *Inorg. Chem.* **2003**, *42*, 5707-5714; (b) Argouarch, G.; Grelaud, G.; Roisnel, T.; Humphrey, M. G.; Paul, F. [Fp*Fc][PF6]: A Remarkable Non-symmetric Dinuclear Cation in a Very Stable Mixed-Valent State will be published in Journal of Organometallic Chemistry, *J. Organomet. Chem.* **2017**, *847*, 218-223.

(57) Gauthier, N.; Argouarch, G.; Paul, F.; Toupet, L.; Ladjarafi, A.; Costuas, K.; Halet, J.-F.; Samoc, M.; Cifuentes, M. P.; Corkery, T. C.; Humphrey, M. G. Electron-rich Iron-Ruthenium Arylalkynyl Complexes for Third-Order Nonlinear Optics. Redox-Switching between Three States, *Chem. Eur. J.* **2011**, *17*, 5561-5577.

(58) Paul, F.; Toupet, L.; Roisnel, T.; Hamon, P.; Lapinte, C. Solid State Characterisation of the [(κ^2-dppe)(η^5-C_5Me_5)FeCO]$^+$ cation: An unexpected "Oxidation" Product of the [(κ^2-dppe)(η^5-C_5Me_5)FeCC(C_6H_4)NMe_2]$^+$ Radical Cation, *C. R. Chim.* **2005**, *8*, 1174-1185 and refs therein.

(59) See for instance: Rebane, A.; Drobizhev, M.; Makarov, N. S.; Beuerman, E.; Haley, J. E.; Krein, D. M.; Burke, A. R.; Flikkema, J. L.; Cooper, T. M. Relation between Two-Photon Absorption and Dipolar Properties in a Series of Fluorenyl-Based Chromophores with Electron Donating or Electron Withdrawing Substituents, *J. Phys. Chem. A* **2011**, *115*, 4255-4262.

(60) Kasha, M. ("Kasha's rule") Characterization of electronic transitions in complex molecules, *Faraday Soc. Discuss.* **1950**, 14-19.

(61) Demchenko, A. P.; Tomin, V. I.; Chou, P.-T. Breaking the Kasha Rule for More Efficient Photochemistry, *Chem. Rev. 2017* **2017**, *117*, 13353-13381.

(62) (a) Zhao, P.; Tofighi, S.; O'Donnell, R. M.; Shi, J.; Zavalij, P. Y.; Bondar, M. V.; Hagan, D. J.; Van Stryland, E. W. Electronic Nature of New Ir(III) Complexes: Linear Spectroscopic and Nonlinear Optical Properties, *Phys. Chem. C* **2017**, *121*, 23609-23617; (b) Kim, K.-Y.; Shelton, A. H.; Drobizhev, M.; Makarov, N.; Rebane, A.; Schanze, K. S. Optimizing Simultaneous Two-Photon Absorption and Transient Triplet-Triplet Absorption in Platinum Acetylide Chromophores, *J. Phys. Chem. A* **2010**, *114*, 7003-7013.

(63) D'Amico, C.; Lorenc, M.; Collet, E.; Green, K. A.; Costuas, K.; Mongin, O.; Blanchard-Desce, M.; Paul, F. Probing Charge-Transfer Excited States in a Quasi Non-Luminescent Electron-Rich Fe(II)-Acetylide Complex by Femtosecond Optical Spectroscopy, *J. Phys. Chem. C* **2012**, *116*, 3719-3727.

(64) Considering the strong luminescence of fluorene-containing organic fluorophores,[59] the assignment of the detected LC-based fluorescence as an artifact originating from traces of organic decomposition products cannot be strictly excluded. However, significant decomposition seems unlikely given the apparent constancy over time of the absorption spectra for both the M(II) (M = Fe, Ru) and Fe(III) complexes during fluorescence measurements. Furthermore, and contrary to Fe(II)

complexes, Ru(II) complexes are perfectly air-stable in their GS and thus not liable to react with adventitious traces of oxygen that might be present in the solvents used.

(65) Marcus, R. A.; Sutin, N. Electron transfers in chemistry and biology, Biophys. Acta 1985, 811, 265-322.

(66) Gatri, R.; Ouerfelli, I.; Efrit, M. L.; Serein-Spirau, F.; Lère-Porte, J.-P.; Valvin, P.; Roisnel, T.; Bivaud, S.; Akdas-Kilig, H.; Fillaut, J.-L. Supramolecular Ruthenium−Alkynyl Multicomponent Architectures: Engineering, Photophysical Properties, and Responsiveness to Nitroaromatics, *Organometallics* **2014**, *33*, 665-676.

(67) Englman, R.; Jortner, J. Mol. Phys. 1970, 18, 145; Wilson, J. S.; Chawdhury, N.; Ai-Mandhary, M. R. A.; Younus, M.; Khan, M. S.; Raithby, P. R.; Köhler, A.; Friend, R. H. J. Am. Chem. Soc. 2001, 123, 9412 (a) Englman, R.; Jortner, J. The energy gap law for radiationless transitions in large molecules, *Mol. Phys.* **1970**, *18*, 145-164; (b) Wilson, J. S.; Chawdhury, N.; Ai-Mandhary, M. R. A.; Younus, M.; Khan, M. S.; Raithby, P. R.; Köhler, A.; Friend, R. H. The energy gap law for triplet states in Pt-containing conjugated polymers and monomers, *J. Am. Chem. Soc.* **2001**, *123*, 9412-9417 and refs therein.

(68) Chou, P.-T.; Chi, Y.; Chung, M.-W.; Lin, C.-C. Harvesting luminescence via harnessing the photophysical properties of transition metal complexes, *Coord. Chem. Rev.* **2011**, *255*, 2653-2665.

(69) Pawlicki, M.; Collins, H. A.; Denning, R. G.; Anderson, H. L. Two-Photon Absorption and the Design of Two-Photon Dyes, *Angew. Chem. Int. Ed.* **2009**, *48*, 3244-3266.

(70) See for instance: Albota, M. A.; Xu, C.; Webb, W. W. Two-photon fluorescence excitation cross sections of biomolecular probes from 690 to 960 nm, *Appl. Opt.* **1998**, *37*, 7352-7356.

(71) Massue, J.; Olesiak-Banska, J.; Jeanneau, E.; Aronica, C.; Matczyszyn, K.; Samoc, M.; Monnereau, C.; Andraud, C. Remarkable Effect of Iridium Cyclometalation on the Nonlinear Absorption Properties of a Quadrupolar Imine Ligand, *Inorg. Chem.* **2013**, *52*, 10705-10707.

(72) Humphrey, M. G.; Schwich, T.; West, P. J.; Cifuentes, M. P.; Samoc, M. Nonlinear Optical Properties of Coordination and Organometallic Complexes in Comprehensive Inorganic Chemistry II - from Element to Applications; Reedijk, J., Poeppelmeier, K., Eds.; Oxford: Elsevier: 2013; Vol. 8, p 781-835.

(73) Shriver, D. F.; Drezdzon, M. A. The Manipulation of Air-Sensitive Compounds; Wiley and sons: New-York, 1986.

(74) Paul, F.; Bondon, A.; da Costa, G.; Malvolti, F.; Sinbandhit, S.; Cador, O.; Costuas, K.; Toupet, L.; Boillot, M.-L. Topological Dependence of the Magnetic Exchange Coupling in Arylethynyl-bridged Organometallic Diradicals containing [(κ^2-dppe)(η^5-C_5Me_5) FeIII]+ Fragments, *Inorg. Chem.* **2009**, *48*, 10608-10624.

(75) Connelly, N. G.; Geiger, W. E. Chemical Redox Agents for Organometallic Chemistry, *Chem. Rev.* **1996**, *96*, 877-910.

(76) Still, W. C.; Kahn, M.; Mitra, A. Rapid chromatographic technique for preparative separations with moderate resolution, *J. Org. Chem.* **1978**, *43*, 2923-2925.

(77) Chen, L. S.; Chen, G. J.; Tamborski, C. 1,3,5-Trisubstituted benzenes. I. Synthesis and reactions of 3,5-dibromophenyllithium, *J. Organomet. Chem.* **1981**, *215*, 281-291.

(78) Smith, A. P.; Lamba, J. J. S.; Fraser, C. L. A convenient LDA Preparation, *Org. Synth.* 2002, *78*, 82-87.

(79) Kofron, W. G.; Baclawski, L. M. A convenient method for estimation of alkyllithium concentrations, *J. Org. Chem.* **1976**, *41*, 1879-1880.

(80) Roger, C.; Hamon, P.; Toupet, L.; Rabaâ, H.; Saillard, J.-Y.; Hamon, J.-R.; Lapinte, C. Halo- and Alkyl(pentamethylcyclo-pentadienyl)(1,2-bis(diphenylphosphino)-ethane)iron(III) 17-Electron Complexes: Synthesis, NMR and Magnetic properties, and EHMO Calculations, *Organometallics* **1991**, *10*, 1045-1054.

(81) Morshedi, M.; Simpson, P. V.; Babgi, B.; Green, K. A.; Moxey, G. J.; Jennaway, M. S.; Cifuentes, M. P.; Humphrey, M. G. cis-tetrakis(dimethyl sulfoxide)ruthenium(II) dichloride, cis-bis{1,2-bis(diphenylphosphino)ethane}ruthenium(II) dichloride, bis{1,2-bis(diphenylphosphino)eth-ene}chloro-ruthenium(II) hexafluoro-phosphate and trans-bis{1,2-bis(diphenylphosphino)ethane}-ruthenium(II) dichloride In *Inorg. Synth.* 2018; Vol. 37, p 171-177.

(82) Doisneau, G.; Balavoine, G.; Fillebeen-Khan, T. Synthesis and some reactions of ferrocenylacetylenes, *J. Organomet. Chem.* **1992**, *425*, 113-117.

(83) (a) Demas, N.; Crosby, G. A. Measurement of photoluminescence quantum yields, *J. Phys. Chem.* **1971** *75*, 991; (b) Eaton, D. F. Reference Materials for Fluorescence Measurment, *Pure Appl. Chem.* **1988**, *60*, 1107-1114.

(84) Duff, C. M.; Heath, G. A. Stepwise Ligand-Additivity Effects on Electrode Potentials and Charge-Transfer Spectra in Hexahalide, Mixed Halide/Nitrile, and Hexakis(nitrile) Complexes of Ruthenium(IV), -(III), and -(II), *Inorg. Chem.* **1991**, *30*, 2528-2535.

(85) Neese, F. The ORCA program system, *Wiley Interdiscip. Rev. Comput. Mol. Sci.* **2012** *2*, 73-78.

(86) (a) Reiher, M.; Salomon, O.; Hess, B. A. Reparameterization of hybrid functionals based on energy differences of states of different multiplicity, *Theor. Chem. Acc.* **2001** *107*, 48-55; (b) Reiher, M. Theoretical Study of the $Fe(phen)_2(NCS)_2$ Spin-Crossover Complex with Reparametrized Density Functionals, *Inorg. Chem.* **2002** *41*, 6928-6935.

(87) Weigend, F.; Ahlrichs, R. Balanced basis sets of split valence, triple zeta valence and quadruple zeta valence quality for H to Rn: Design and assessment of accuracy, *Phys. Chem. Chem. Phys.* **2005**, *7*, 3297-3305.

(88) (a) Grimme, S.; Ehrlich, S.; Goerigk, L. Effect of the damping function in dispersion corrected density functional theory, *J. Comput. Chem.* **2011**, *32*, 1456-1465; (b) Grimme, S.; Antony, J.; Ehrlich,

S.; Krieg, H. J. A consistent and accurate ab initio parametrization of density functional dispersion correction (DFT-D) for the 94 elements H-Pu, *Chem. Phys.* **2010**, *132*, 154104(1-19).

(89) van Wüllen, C. J. Molecular density functional calculations in the regular relativistic approximation: method, application to coinage metal diatomics, hydrides, fluorides and chlorides, and comparison with first-order relativistic calculations, *J. Chem. Phys.* **1998**, *109*, 392-399.

(90) (a) Harvey, J. N. Spin-forbidden reactions: computational insight into mechanisms and kinetics, *Wiley Interdiscip. Rev. Comput. Mol. Sci.* **2014**, *4*, 1-14; (b) Harvey, J. N.; Aschi, M.; Schwarz, H.; Koch, W. The singlet and triplet states of phenyl cation. A hybrid approach for locating minimum energy crossing points between non-interacting potential energy surfaces, *Theor. Chem. Acc.* **1998**, *99*, 95-99.

(91) Allouche, A.-R. Gabedit-A graphical user interface for computational chemistry softwares, *J. Comput. Chem.* **2011**, *32*, 174-182.

(92) Merhi, A.; Grelaud, G.; Ripoche, N.; Barlow, A.; Cifuentes, M. P.; Humphrey, M. G.; Paul, F.; Paul-Roth, C. O. A Zinc(II) Tetraphenylporphyrin Peripherally Functionalized with Redox-Active "trans-[(η^5-C_5H_5)Fe(η^5-C_5H_4)-C≡C](κ^2-dppe)$_2$Ru(C≡C)-" Substituents: Linear Electro-chromism and Third-Order Nonlinear Optics, *Polyhedron* **2015**, *86*, 64-70.

(93) Sheikh-Bahae, M.; Said, A. A.; Wei, T.; Hagan, D. J.; Stryland, E. W. V. Sensitive measurement of optical nonlinearities using a single beam, *IEEE J. Quant. Electr.* **1990**, *26*, 760-769.

(94) Blessing, R. H. An empirical correction for absorption anisotropy, *Acta Cryst.* **1995**, *A51*, 33-38.

(95) Sheldrick, G. M. A short history of SHELX, *Acta Crystallogr. A* **2008**, *64*, 112-122.

(96) Sheldrick, G. M. Crystal structure refinement with SHELXL, *Acta Crystallogr. C* **2015**, *71*, 3-8.

(97) Dolomanov, O. V.; Bourhis, L. J.; Gildea, R. J.; Howard, J. A. K.; Puschmann, H. OLEX2: a complete structure solution, refinement and analysis program, *J. Appl. Cryst.* **2009**, *42*, 339-341.

(98) Reidel, D. *International Tables for X-ray Crystallography*; Kynoch Press (present distrib. D. Reidel, Dordrecht): Birmingham, 1974; Vol. IV.

(99) Farrugia, L. J. WinGX and ORTEP for Windows: an update, *J. Appl. Crystallogr.* **2012**, *45*, 849-854.